Sphinx Journal of Mathematical Sciences
1(2), 1–27, 2026
DOI: https://doi.org/10.64389/sjms.2026.012116
https://sphinxsp.org/journal/index.php/sjms/

Research article

Stochastic and Initial Stress Effects on Wave Propagation in Micro-elongated Thermoelastic Media under the Refined Dual-Phase-Lag Model With Multiplicative White Noise

M. Elsaid Ramadan[1,*], **Mohamed A. El-bassiouny**[2]

[1] Department of Mathematics, Faculty of Science, Islamic University of Madinah, Medina, Saudi Arabia.

[2] Department of Mathematics and Computer Science, Faculty of Science, Alexandria University, Alexandria, Egypt.

* **Correspondence:** m.elsaid@iu.edu.sa

ARTICLE INFO

Keywords:
Refined Dual-Phase-Lag Model;
Micro-elongated Stochastic;
Stochastic system;
Initial Stress

Mathematics Subject Classification:
74A15, 74A18, 93E03.

Important Dates:
Received: 1 May 2026
Revised: 28 May 2026
Accepted: 1 June 2026
Online: 2 June 2026

Copyright © 2025 by the authors. Published under Creative Commons Attribution (CC BY) license.

ABSTRACT

This work provides an in-depth investigation of the influence of initial stress on wave propagation phenomena within a micro-elongated stochastic thermoelastic medium with the Lord-Shulman theory (LST), the Dual-Phase-Lag Model (DPLM), and the Refined Dual-Phase-Lag Model (RDPLM). Through an appropriate nondimensionalization procedure combined with a suitable transform technique, the initially complex system of coupled stochastic partial differential equations is systematically transformed into a set of stochastic ordinary differential equations for which explicit analytical solutions can be obtained. The obtained solutions offer a comprehensive understanding of the dynamic response of the medium, including the displacement components, the evolution of micro-elongation, the induced stress fields, and the associated temperature variations. Consequently, the proposed framework delivers a complete and coherent description of thermo-mechanical wave behavior in the presence of initial stress. In addition, extensive numerical simulations are carried out to compare deterministic predictions with their stochastic analogues. These comparisons clearly demonstrate how initial stress effects and random thermal fluctuations significantly modify wave characteristics, such as amplitude, attenuation, and propagation patterns, thereby emphasizing the critical role of stochasticity in realistic thermoelastic wave modeling.

1. Introduction

Stochastic thermoelasticity represents a modern development of both classical and generalized thermoelastic theories by incorporating probabilistic effects into the mathematical description of thermo-mechanical behavior. Unlike deterministic formulations, which assume that all material parameters, external loads, and environmental conditions are perfectly known, stochastic models recognize that real engineering systems are inevitably affected by numerous sources of uncertainty. These uncertainties may originate from random variations in material properties, microscopic defects, manufacturing inconsistencies, experimental errors, thermal fluctuations, unpredictable environmental influences, and randomly varying mechanical or thermal excitations. Since these factors can significantly influence the response of thermoelastic media, deterministic models may provide only approximate predictions that fail to accurately represent the actual physical behavior observed in practice. To overcome these limitations, stochastic thermoelastic formulations explicitly introduce random effects into the governing equations, particularly the heat conduction equation. This is generally achieved by incorporating stochastic variables or random forcing terms that describe uncertain thermal disturbances. Common mathematical representations include Wiener stochastic processes [8], Gaussian white-noise excitations, and other random perturbation models [9, 15]. The inclusion of such stochastic components transforms the governing equations into probabilistic models capable of describing both deterministic trends and random fluctuations within the thermoelastic response. A major advantage of this probabilistic framework is that it provides considerably more information than conventional deterministic analyses. Rather than computing only a single predicted solution, stochastic thermoelasticity evaluates the statistical characteristics of the response, including expected values, variances, probability distributions, and the temporal evolution of uncertainty. As a consequence, important physical variables such as displacement, temperature, stress, and strain are interpreted as random fields whose behavior depends not only on the deterministic material constants and loading conditions but also on the statistical properties and intensity of the imposed stochastic disturbances [27, 4]. This approach enables a more comprehensive understanding of the influence of uncertainty on thermo-mechanical wave propagation and heat transfer. Extensive theoretical developments and practical applications of stochastic thermoelasticity have been presented in the literature [28, 23]. The theory has proven particularly effective for analyzing advanced engineering materials and complex physical systems where random effects cannot be neglected. Typical applications include composite materials, porous structures, functionally graded materials, microstructured solids, biological tissues, and thermoelastic systems exposed to irregular or fluctuating thermal environments. In these situations, stochastic formulations successfully capture important physical phenomena, including uncertainty-induced attenuation, random fluctuations in thermal and mechanical fields, altered wave propagation characteristics, and modifications in dispersion behavior. Consequently, stochastic thermoelasticity has become an essential analytical framework for improving predictive accuracy, enhancing structural reliability, and supporting the safe design of engineering components operating under uncertain service conditions [24, 26].

The RDPLM represents a significant advancement in non-Fourier heat conduction theories, developed specifically to address the inherent limitations of the conventional DPLM. Although the DPLM accounts for finite thermal propagation by introducing two relaxation times associated with the phase lags of heat flux and temperature gradient, it has been shown to be insufficient for accurately describing ultra-fast thermal processes encountered in modern micro-scale applications. To overcome these deficiencies, the RDPLM extends the classical DPLM through the incorporation of higher-order correction terms and a more rigorous characterization of the phase-lag parameters within the constitutive heat-conduction equation [30, 19].

These refinements enhance the physical realism of the model by providing a more accurate representation of finite-speed heat transfer mechanisms. Consequently, the RDPLM is capable of capturing wave-like thermal transport phenomena, in which heat propagation occurs with measurable delays rather than instantaneous diffusion [1, 21]. This improved formulation effectively resolves several shortcomings associated with the standard DPLM, including non-physical instabilities and unrealistic predictions of temperature overshoots or peak values that commonly arise under conditions of ultra-fast thermal excitation [31, 10]. By eliminating these anomalies, the RDPLM yields stable and physically consistent thermal responses. Detailed discussions of the theoretical development and practical implications of the RDPLM can be found in [7, 13]. Owing to these advantages, the RDPLM has gained increasing attention in the analysis of thermoelastic behavior, particularly in micro-scale systems. Micro-elongated thermoelastic materials represent an important subclass of generalized continuum theories that extend the limitations of classical thermoelasticity by incorporating the influence of the material's internal microstructure into the mathematical formulation [2, 22]. Unlike conventional thermoelastic models, which assume that the mechanical behavior of a material is completely characterized by the macroscopic displacement field together with the temperature distribution, the micro-elongated theory introduces an additional independent kinematic variable associated with microscopic elongation or stretch. This supplementary degree of freedom enables the continuum to describe deformation processes occurring at the microstructural level that cannot be represented within the framework of classical elasticity. The concept of micro-elongation is intended to capture the local extension experienced by the material's internal constituents, including microscopic fibers, molecular networks, granular inclusions, cellular elements, or other embedded structural components. Such internal stretching mechanisms arise naturally in numerous heterogeneous and composite materials, where the microstructural elements are capable of deforming independently of the surrounding matrix. Consequently, the overall mechanical behavior is no longer governed solely by macroscopic displacement but also depends on the evolution of these internal deformation modes. By accounting for these additional microstructural effects, the micro-elongated continuum provides a significantly richer and more realistic description of material behavior, particularly in situations where microscopic interactions have a measurable impact on the observable macroscopic response [14, 12]. From a physical perspective, the inclusion of the micro-elongation variable allows the theory to represent the storage and transfer of energy associated with internal stretching mechanisms that are completely neglected in classical thermoelastic formulations. These microscopic deformation processes introduce additional internal forces and moments that alter the stress field throughout the material. As a consequence, the constitutive equations become more comprehensive by incorporating coupling terms between the conventional displacement field, the micro-elongation variable, and the thermal field. This enhanced theoretical framework is especially suitable for describing the behavior of modern engineering materials possessing complex internal architectures, including fiber-reinforced composites, porous solids, polymeric materials, biological tissues, cellular structures, nano-engineered materials, and various multifunctional composites whose mechanical characteristics are strongly influenced by their internal morphology. When thermal effects are incorporated into the analysis, the interaction between heat conduction and microstructural deformation becomes considerably more intricate. Temperature variations not only generate conventional thermoelastic strains but also influence the microscopic elongation of the internal structural elements. Conversely, the evolution of the micro-elongation field modifies the thermal response through additional coupling mechanisms, thereby affecting the distribution of temperature, the generation of thermal stresses, and the transport of thermal energy. These mutual interactions produce constitutive relations that are substantially more sophisticated than those found in classical thermoelasticity, since the governing equations must simultaneously describe the evolution of macroscopic displacement, temperature, and microscopic elongation while preserving the energetic consistency of the continuum [5]. The presence of these coupled microstructural and thermal mechanisms has a profound influence on the dynamic response of the material. In particular, elastic and thermoelastic waves propagating through micro-elongated media exhibit characteristics that differ substantially from those predicted by traditional continuum theories. The additional internal degree of freedom gives rise to new wave modes and significantly modifies the propagation of existing mechanical and thermal disturbances. Phenomena such as frequency-dependent dispersion, enhanced attenuation, internal relaxation, delayed energy transfer, and complex wave interactions naturally emerge as direct consequences of the microstructural deformation mechanisms. Furthermore, the stress distribution and temperature evolution become highly sensitive to the material's internal characteristics, including the stiffness associated with microscopic stretching, the coupling coefficients between thermal and mechanical fields, and the geometric configuration of the microstructure. Extensive theoretical and numerical investigations reported in the literature have demonstrated that these microstructural effects become increasingly significant in materials possessing pronounced internal heterogeneity or operating under high-frequency dynamic loading conditions [16, 17]. Owing to its ability to incorporate internal deformation mechanisms beyond the scope of classical elasticity, the theory of micro-elongated thermoelasticity has become an indispensable modeling framework for the analysis of coupled thermo-mechanical phenomena in advanced materials. It provides a rigorous mathematical basis for investigating the influence of microscopic stretching on stress generation, heat transfer, and wave propagation while offering improved predictive capability for materials whose behavior is governed by interactions occurring across multiple length scales. Consequently, the micro-elongated thermoelastic model serves as a powerful and physically consistent approach for studying modern microstructured materials in engineering, materials science, biomechanics, and related interdisciplinary applications where conventional thermoelastic theories are insufficient to accurately represent the observed physical behavior.

Initial stress represents one of the most significant parameters in generalized thermoelasticity because many engineering materials and structural systems do not begin their operational life in a completely unstressed configuration. Instead, they frequently possess pre-existing stress fields that develop before the application of subsequent mechanical forces or thermal disturbances. These residual or initial stresses may arise during manufacturing operations, welding procedures, casting, rolling, machining, heat treatment, assembly processes, differential thermal expansion, or prolonged exposure to mechanical and environmental loading throughout the service life of a component. Since these stresses already exist within the material prior to any additional excitation, they substantially influence its subsequent mechanical and thermal behavior and therefore cannot be neglected in realistic thermoelastic analyses. From a theoretical standpoint, the presence of an initial stress field changes the reference equilibrium state of the continuum, thereby modifying the governing equations that describe the coupled interaction between displacement, strain, temperature, and stress. Unlike stress-free media, where the constitutive behavior depends only on the current deformation and thermal fields, pre-stressed materials exhibit additional coupling effects because the initial stress contributes directly to the incremental response of the medium. Consequently, the constitutive equations become more complex, incorporating the influence of the pre-existing stress state into both the mechanical and thermal balance equations. This modification results in a more accurate mathematical representation of the physical processes occurring inside materials subjected to realistic loading histories [11, 20]. The influence of initial stress becomes particularly evident in the propagation of thermoelastic waves. Since wave motion depends strongly on the stiffness characteristics of the medium, the existence of pre-stress alters the effective elastic properties experienced by propagating disturbances. Depending on whether the initial stress is tensile or compressive, as well as its magnitude and direction, the propagation velocities of both elastic and thermal waves may either increase or decrease. Moreover, initial stress can modify the trajectories of propagating waves, alter their reflection and transmission characteristics at material interfaces, and significantly influence the spatial distribution of stresses generated during dynamic loading. These effects are especially important in structures operating under severe mechanical environments, where relatively small changes in the initial stress state may produce substantial variations in the overall dynamic response of the material. Another important consequence of incorporating initial stress is the emergence of anisotropic behavior in materials that are intrinsically isotropic under unstressed conditions. The preferred direction introduced by the pre-existing stress field breaks the original material symmetry, causing the propagation characteristics to become direction dependent. As a result, wave velocities, attenuation coefficients, and dispersion characteristics vary according to the orientation of propagation relative to the principal directions of the initial stress. This stress-induced anisotropy has attracted considerable attention because it provides a realistic explanation for many experimentally observed phenomena that cannot be adequately described using conventional isotropic thermoelastic models [18, 3]. In addition to modifying wave propagation, initial stress also affects the mechanisms responsible for energy transport and thermo-mechanical coupling. The interaction between residual stress and temperature variations introduces additional pathways for energy conversion between mechanical deformation and thermal processes. These coupling effects become increasingly pronounced under conditions involving rapid heating, transient thermal shocks, pulsed heat sources, or high-frequency dynamic excitations, where the evolution of the thermal and mechanical fields occurs over very short time scales. Under such circumstances, the initial stress influences not only the magnitude of the generated stresses but also the evolution of the temperature field, heat flux distribution, and internal energy dissipation. Consequently, neglecting the contribution of pre-existing stresses may lead to inaccurate predictions of the material response, particularly in advanced thermoelastic models that seek to describe finite-speed heat propagation and non-classical thermal relaxation phenomena. Because of these significant physical effects, incorporating initial stress into thermoelastic formulations provides a substantially more realistic and comprehensive description of the behavior of engineering materials under practical operating conditions. The resulting mathematical models are capable of capturing the combined influence of mechanical preloading, thermal excitation, and microstructural interactions, thereby improving the predictive accuracy of stress analysis, temperature evolution, and dynamic wave propagation. Such enhanced modeling frameworks have become indispensable in numerous scientific and technological fields, including geomechanics, earthquake engineering, aerospace engineering, structural health monitoring, biomechanics, civil infrastructure, energy systems, and the development of advanced multifunctional and microstructured materials. In these applications, the existence of residual or operational stresses often governs the structural integrity, fatigue resistance, vibration characteristics, and long-term thermo-mechanical performance of the material, making the inclusion of initial stress an essential requirement for reliable theoretical and computational analyses [29].

This study examines the combined impact of initial stress and stochastic disturbances on the thermoelastic response of a micro-elongated half-space, within the theoretical frameworks of the LST, the DPLM, and its refined variant, the RDPLM. The analysis commences with the formulation of the fundamental governing equations that characterize the coupled interactions among mechanical deformation, heat transfer, and micro-elongation within the medium. To facilitate an efficient and systematic analytical treatment, the governing equations are recast in a dimensionless form. Subsequently, by employing the transform specified in Eq. (3.1), the original system of coupled stochastic partial differential equations is rigorously reduced to a tractable set of stochastic ordinary differential equations. The application of the prescribed boundary conditions at $z = 0$ enables the evaluation of the unknown constants, thereby completing the analytical solution procedure. The derived solutions are then utilized to conduct extensive numerical computations and graphical investigations. These results offer detailed insight into how initial stress and stochastic excitation influence the spatial behavior of key physical fields, including displacement, temperature, stress components, and micro-elongation, within the micro-elongated thermoelastic medium.

2. Governing Equations

This section introduces the governing equations for two-dimensional micro-elongated stochastic thermoelasticity within the LST, DPLM, and RDPLM , with particular attention to the effect of initial stress. To simplify the analysis, the equations are subsequently reformulated in a dimensionless form.
The equation of motion can be written as:

$$\sigma_{ij,i} = \rho u_{i,tt}, \tag{2.1}$$

where

$$\sigma_{ij} = (\lambda e - \beta_0 \vartheta + \lambda_0 \psi - P)\,\delta_{ij} + 2\mu\varepsilon_{ij} - \frac{P}{2}\left(u_{j.i} - u_{i,j}\right). \tag{2.2}$$

The equation of micro-elongated can be given as:

$$a_0\psi_{,ii} - \lambda_1\psi + \beta_1\vartheta - \lambda_0 u_{j,j} = \frac{\rho j^* \psi_{,tt}}{2}. \tag{2.3}$$

The energy equation can be expressed as follows [12]:

$$\begin{aligned} 0 \;=\;& k\left(1 + \Sigma_{m=1}^{M}\frac{\tau_\theta^m}{(m)!}\frac{\partial^m}{\partial t^m}\right)\vartheta_{,ii} - \beta_1 T_0 \psi_{,t} + \frac{\nu\vartheta_{,x}}{T_0}\frac{dW(t)}{dt} \\ &-\left(1 + \Sigma_{m=1}^{M}\frac{\tau_q^m}{(m)!}\frac{\partial^m}{\partial t^m}\right)\left[\beta_0 T_0\left(u_{,xt} + w_{,zt}\right) + \rho c_e \vartheta_{,t}\right], \end{aligned} \tag{2.4}$$

When
1- $M = 3$ and $(\tau_\theta < \tau_q \neq 0, k \neq 0)$ is RDPM,
2- $M = 1$ and $(\tau_\theta < \tau_q \neq 0, k \neq 0)$ is DPLM,
3- $M = 1$ and $(\tau_\theta = 0, \tau_q \neq 0, k \neq 0)$ is LST.
where, $W(t)$ represents the Wiener process, while $\frac{dW(t)}{dt}$ white noise, and ν denotes the intensity of the white noise acting on the system.
The Wiener process is distinguished by several essential statistical features, which are given below [25, 6]:
i: For $t > \iota$, $W(t) - W(\iota)$ has independent increments.
ii: For $t \geq 0$, $W(t)$ has continuous trajectories.
iii: $W(t) - W(\iota)$ has a normal distribution with variance $= t - \iota$ and mean $= 0$.
Utilizing Eq. (2.2) in Eq. (2.1) with the aid of the displacement vector $\mathbf{u}(x, z, t) = u(u, 0, w)$, we see

$$\mu\nabla^2 u + (\lambda + \mu)\,e_{,x} - \beta_0\vartheta_{,x} + \lambda_0\psi_{,x} + \frac{P}{2}\left(u_{,zz} - w_{,xz}\right) = \rho u_{,tt}, \tag{2.5}$$

$$\mu\nabla^2 w + (\lambda + \mu)\,e_{,z} - \beta_0\vartheta_{,z} + \lambda_0\psi_{,z} + \frac{P}{2}\left(w_{,xx} - u_{,xz}\right) = \rho w_{,tt}. \tag{2.6}$$

Employing the displacement vector $\mathbf{u}(x,z,t) = u(u,0,w)$ in Eq. (2.3), one infers

$$a_0\psi_{,ii} + \beta_1\vartheta - \lambda_1\psi - \lambda_0\left(u_{,x} + w_{,z}\right) = \frac{\rho j^*\psi_{,tt}}{2}. \tag{2.7}$$

For the purpose of the present investigation, an appropriate set of dimensionless variables is introduced to reformulate the governing equations into a non-dimensional framework. This transformation not only reduces the number of physical parameters involved but also simplifies the mathematical expressions, thereby facilitating the analytical treatment of the problem. Furthermore, the dimensionless formulation provides a clearer interpretation of the underlying physical mechanisms and enables a more systematic examination of the thermo-mechanical behavior of the system under various operating conditions.

$$\begin{aligned}(u,\ v) &= \frac{T_0\beta_0}{\rho c_1\omega^*}\left(\bar{u},\ \bar{v}\right),\ (x,z) = \frac{c_1}{\omega^*}\left(\bar{x},\ \bar{z}\right),\ \vartheta = T_0\bar{\vartheta},\ \left(t,\ \tau_\theta,\ \tau_q\right) = \frac{\left(\bar{t},\ \bar{\tau}_\theta,\ \bar{\tau}_q\right)}{\omega^*},\ \sigma_{ij} = \beta_1 T_0\bar{\sigma}_{ij},\\ p &= (\lambda + 2\mu)\bar{P},\ \psi = \frac{\beta_0 T_0}{\lambda_0}\bar{\psi},\ k\omega^* = \rho c_1^2 c_e,\ \rho c_1^2 = \lambda + \mu.\end{aligned} \tag{2.8}$$

Using Eq. (2.8) in Eq. (2.5), one acquires

$$\left(b_1\nabla^2 - \frac{\partial^2}{\partial t^2} + b_2\frac{\partial^2}{\partial x^2} + \frac{P}{2}\frac{\partial^2}{\partial z^2}\right)u + \left(b_2 - \frac{P}{2}\right)\frac{\partial^2 w}{\partial x\partial z} - \frac{\partial\vartheta}{\partial x} + \frac{\partial\psi}{\partial x} = 0, \tag{2.9}$$

Implementing Eq. (2.8) in Eq. (2.6), we discover

$$\left(b_2 - \frac{P}{2}\right)\frac{\partial^2 u}{\partial x\partial z} + \left(b_1\nabla^2 - \frac{\partial^2}{\partial t^2} + b_2\frac{\partial^2}{\partial z^2} + \frac{P}{2}\frac{\partial^2}{\partial x^2}\right)w - \frac{\partial\vartheta}{\partial z} + \frac{\partial\psi}{\partial z} = 0, \tag{2.10}$$

Applying Eq. (2.8) in Eq. (2.7), one realizes

$$b_5\frac{\partial u}{\partial x} + b_5\frac{\partial w}{\partial z} - b_3\vartheta - \left(\nabla^2 - b_4 - b_6\frac{\partial^2}{\partial t^2}\right)\psi = 0, \tag{2.11}$$

Inserting Eq. (2.8) in Eq. (2.4), we find

$$b_8\left(1+\tau_2\right)\frac{\partial^2 u}{\partial x\partial t} + b_8\left(1+\tau_2\right)\frac{\partial^2 w}{\partial z\partial t} - \left(\nabla^2 + \tau_1\nabla^2 - b_7\frac{\partial}{\partial t} - \tau_2 b_7\frac{\partial}{\partial t}\right)\vartheta + \frac{\nu c_1}{kT_0\omega^*}\frac{\partial\vartheta}{\partial x}\frac{dW(t)}{dt} + b_9\frac{\partial\psi}{\partial t} = 0, \tag{2.12}$$

where, $b_1 = \frac{\mu}{c_1^2\rho}$, $b_2 = \frac{\mu+\lambda}{c_1^2\rho}$, $b_3 = \frac{\lambda_0\beta_1 c_1^2}{\beta_0 a_0\omega^{*2}}$, $b_4 = \frac{c_1^2\lambda_1}{a_0\omega^{*2}}$, $b_5 = \frac{\lambda_0^2}{a_0\rho\omega^{*2}}$, $b_6 = \frac{\rho j^* c_1^2}{2a_0}$, $b_7 = \frac{\rho c_e c_1^2}{k\omega^*}$, $b_8 = \frac{\beta_0^2 T_0}{k\omega^*\rho}$, $b_9 = \frac{\beta_0\beta_1 T_0 c_1^2}{k\omega^*\lambda_0}$, $\tau_1 = \Sigma_{m=1}^{M}\frac{\tau_\theta^m}{m!}\frac{\partial^m}{\partial t^m}$, and $\tau_2 = \Sigma_{m=1}^{M}\frac{\tau_q^m}{m!}\frac{\partial^m}{\partial t^m}$.
Using Eq. (2.8) in Eq. (2.2), we have

$$\sigma_{xx} = \frac{\partial u}{\partial x} + b_{10}\frac{\partial w}{\partial z} - \vartheta + \psi - b_{11}P, \tag{2.13}$$

$$\sigma_{zz} = b_{10}\frac{\partial u}{\partial x} + \frac{\partial w}{\partial z} - \vartheta + \psi - b_{11}P, \tag{2.14}$$

$$\sigma_{zx} = \sigma_{xz} = b_{12}\frac{\partial u}{\partial z} + b_{13}\frac{\partial w}{\partial x}. \tag{2.15}$$

where, $b_{10}=\frac{\lambda_0^2}{a_0\rho\omega^{*2}}$, $b_{11}=\frac{\lambda+2\mu}{\beta_0 T_0}$, $b_{12}=\frac{\mu+(\lambda+2\mu)\frac{P}{2}}{c_1^2\rho}$, $b_{13}=\frac{\mu-(\lambda+2\mu)\frac{P}{2}}{c_1^2\rho}$.
The displacement potentials $\xi(x,\ z,\ t)$ and $\eta(x,\ z,\ t)$ which relate to displacement components have been introduced,one receives

$$u=\xi_{,x}+\eta_{,z},\qquad w=\xi_{,z}-\eta_{,x}. \tag{2.16}$$

Using Eq. (2.16) in Eqs. (2.9), (2.10), (2.11), and (2.12), we acquire

$$\left[(b_1+b_2)\nabla^2-\frac{\partial^2}{\partial t^2}\right]\xi-\vartheta+\psi=0, \tag{2.17}$$

$$\left[\left(b_1+\frac{P}{2}\right)\nabla^2-\frac{\partial^2}{\partial t^2}\right]\eta=0, \tag{2.18}$$

$$b_5\nabla^2\xi-b_3\vartheta-\left(\nabla^2-b_4-b_6\frac{\partial^2}{\partial t^2}\right)\psi=0, \tag{2.19}$$

$$b_8(1+\tau_2)\nabla^2\left(\frac{\partial\xi}{\partial t}\right)-\left(\nabla^2+\tau_1\nabla^2-b_7\frac{\partial}{\partial t}-\tau_2 b_7\frac{\partial}{\partial t}\right)\vartheta+\frac{vc_1}{kT_0\omega^*}\frac{\partial\vartheta}{\partial x}\frac{dW(t)}{dt}+b_9\frac{\partial\psi}{\partial t}=0. \tag{2.20}$$

3. Solution

The solution for the considered physical variables can be formulated and examined using a modal representation as follows:

$$\left[u,\ w,\ \vartheta,\ \psi,\ \xi,\ \eta,\ \sigma_{ij}\right](x,\ z,\ t)=\left[\tilde{u},\ \tilde{w},\ \tilde{\vartheta},\ \tilde{\psi},\ \tilde{\xi},\ \tilde{\eta},\ \tilde{\sigma}_{ij}\right](z)\,e^{i\left(\varsigma x-\omega t+vW(t)-v^2t\right)}. \tag{3.1}$$

where, ς is the wave number and ω is the frequency
Inserting Eq. (3.1) into Eqs. (2.17), (2.18), (2.19), and (2.20), we get

$$\left(\gamma_1D^2+\gamma_2\right)\tilde{\xi}-\tilde{\vartheta}+\tilde{\psi}=0, \tag{3.2}$$

$$\left[\gamma_3D^2+\gamma_4\right]\tilde{\eta}=0, \tag{3.3}$$

$$\left[b_5D^2-\gamma_5\right]\tilde{\xi}-b_3\tilde{\vartheta}-\left(D^2+\gamma_6\right)\tilde{\psi}=0, \tag{3.4}$$

$$\left[\gamma_7D^2-\gamma_8\right]\tilde{\xi}-\left(\gamma_9D^2-\gamma_{10}\right)\tilde{\vartheta}+\gamma_{11}\tilde{\psi}=0, \tag{3.5}$$

where, $\gamma_1=b_1+b_2$, $\gamma_2=\left(\omega+v^2-v\frac{dW(t)}{dt}\right)^2-\varsigma^2\gamma_1$, $\gamma_3=b_1+\frac{P}{2}$, $\gamma_4=\left(\omega+v^2-v\frac{dW(t)}{dt}\right)^2-b_1\varsigma^2$, $\gamma_5=\varsigma^2b_5$, $\gamma_6=b_6\left(\omega+v^2-v\frac{dW(t)}{dt}\right)^2-b_4-\varsigma^2$, $\gamma_7=ib_8(1+\tau_2)\left(v\frac{dW(t)}{dt}-\omega-v^2\right)$, $\gamma_8=\gamma_7\varsigma^2$, $\gamma_9=(1+\tau_1)$, $\gamma_{10}=\gamma_9\varsigma^2+ib_7(1+\tau_2)\left(\omega+v^2-v\frac{dW(t)}{dt}\right)-\frac{i\varsigma vc_1}{kT_0\omega^*}\frac{dW(t)}{dt}$, $\gamma_{11}=ib_9\left(v\frac{dW(t)}{dt}-\omega-v^2\right)$.
It is observed that the cases

1. $\tau_1=\left(\omega+v^2-v\frac{dW(t)}{dt}\right)\tau_\theta\left[-i-\left(\omega+v^2-v\frac{dW(t)}{dt}\right)\frac{\tau_\theta}{2}+i\left(\omega+v^2-v\frac{dW(t)}{dt}\right)^2\frac{\tau_\theta^2}{6}\right]$ and

   $\tau_2=\left(\omega+v^2-v\frac{dW(t)}{dt}\right)\tau_q\left[-i-\left(\omega+v^2-v\frac{dW(t)}{dt}\right)\frac{\tau_q}{2}+i\left(\omega+v^2-v\frac{dW(t)}{dt}\right)^2\frac{\tau_q^2}{6}\right]$ correspond to the RDPLM

2. $\tau_1=-i\left(\omega+v^2-v\frac{dW(t)}{dt}\right)\tau_\theta$ and $\tau_2=-i\left(\omega+v^2-v\frac{dW(t)}{dt}\right)\tau_q$ correspond to the DPLM

3. $\tau_1 = 0$ and $\tau_2 = -i\left(\omega + \nu^2 - \nu\frac{dW(t)}{dt}\right)\tau_q$ correspond to the LST

Equations (3.2), (3.4), and (3.5) yield a nontrivial solution when the determinant of the coefficient matrix associated with the physical quantities equals zero. Using the MATLAB program, we infer

$$\left(D^6 - B_1 D^4 + B_2 D^2 - B_3\right)\{\tilde{\xi}(z),\ \tilde{\vartheta}(z),\ \tilde{\psi}(z)\} = 0, \tag{3.6}$$

where, $B_1 = \frac{1}{\gamma_1\gamma_9}\{\gamma_7 + \gamma_1\gamma_{10} - \gamma_2\gamma_9 - b_5\gamma_9 - \gamma_1\gamma_6\gamma_9\}$,
$B_2 = \frac{-1}{\gamma_1\gamma_9}\{-\gamma_8 + \gamma_2\gamma_{10} + \gamma_6\gamma_7 + \gamma_5\gamma_9 + \gamma_7 b_3 + \gamma_{10} b_5 + \gamma_{11} b_5 + \gamma_1\gamma_6\gamma_{10} - \gamma_2\gamma_6\gamma_9 - \gamma_1^2\}$,
$B_3 = \frac{1}{\gamma_1\gamma_9}\{-\gamma_8 b_3 - \gamma_6\gamma_8 - \gamma_5\gamma_{10} - \gamma_5\gamma_{11} + \gamma_2\gamma_6\gamma_{10} - \gamma_2\gamma_{11} b_3\}$.
This equation can be written as

$$\left(D^2 - r_1\right)\left(D^2 - r_2\right)\left(D^2 - r_3\right)\{\tilde{\xi}(z),\ \tilde{\vartheta}(z),\ \tilde{\psi}(z)\} = 0, \tag{3.7}$$

where, r_1, r_2, and r_3 are roots
The general solution of Eq. (3.7) bound as $z \to \infty$ can be expressed as

$$\tilde{\xi}(z) = \Sigma_{n=1}^{3} R_n e^{-r_n z}, \tag{3.8}$$
$$\tilde{\psi}(z) = \Sigma_{n=1}^{3} \Theta_{1n} R_n e^{-r_n z}, \tag{3.9}$$
$$\tilde{\vartheta}(z) = \Sigma_{n=1}^{3} \Theta_{2n} R_n e^{-r_n z}, \tag{3.10}$$

where, $\Theta_{1n} = \frac{(b_5 - b_3\gamma_1)r_n^2 - (b_3\gamma_2 + \gamma_5)}{r_n^2 + b_3 + \gamma_6}$, $\Theta_{2n} = \gamma_1 r_n^2 + \gamma_2 + \Theta_{1n}$.
The general solution of Eq. (3.3) bound as $z \to \infty$ can be written as

$$\tilde{\eta}(z) = N e^{-Sz}, \tag{3.11}$$

where $S = \sqrt{\frac{-\gamma_4}{\gamma_3}}$.
Employing Eq. (3.1) in Eq. (2.16), then using Eqs. (3.8) and (3.11), one obtains

$$\tilde{u} = -i\varsigma\Sigma_{n=1}^{3} R_n e^{-r_n z} - S N e^{-Sz}, \tag{3.12}$$
$$\tilde{w} = -\Sigma_{n=1}^{3} r_n R_n e^{-r_n z} + i\varsigma N e^{-Sz}. \tag{3.13}$$

Using Eq. (3.1) into Eqs. (2.13), (2.14), and (2.15), then employing Eqs. (3.9), (3.10), (3.12) and (3.13), one infers

$$\tilde{\sigma}_{xx} = \Sigma_{n=1}^{3} \Theta_{3n} R_n e^{-r_n z} + i\varsigma(1 - b_{10}) S N e^{-Sz} - b_{11} P, \tag{3.14}$$
$$\tilde{\sigma}_{zz} = \Sigma_{n=1}^{3} \Theta_{4n} R_n e^{-r_n z} + i\varsigma(b_{10} - 1) S N e^{-Sz} - b_{11} P, \tag{3.15}$$
$$\tilde{\sigma}_{xz} = \tilde{\sigma}_{zx} = \Sigma_{n=1}^{3} \Theta_{5n} R_n e^{-r_n z} + \left(b_{12} S^2 + b_{13}\varsigma^2\right) N e^{-Sz}, \tag{3.16}$$

where, $\Theta_{3n} = b_{10} r_n^2 - \varsigma^2 + \Theta_{1n} - \Theta_{2n}$, $\Theta_{4n} = r_n^2 - b_{10}\varsigma^2 + \Theta_{1n} - \Theta_{2n}$, $\Theta_{5n} = i\varsigma(b_{12} r_n - b_{13} r_n)$.

4. Boundary condition

To find the constants $(R_1,\ R_2,\ R_3,\ \text{and } N)$, we have applied the boundary conditions for the problem at $z = 0$ as follows:

$$\sigma_{xz} = 0,\ \sigma_{zz} = f_1 e^{i\left(\varsigma x-\omega t+\nu W(t)-\nu^2 t\right)} - b_{11}P,\ \frac{\partial\psi}{\partial z} = 0,\ \vartheta\ = f_2 e^{i\left(\varsigma x-\omega t+\nu W(t)-\nu^2 t\right)}, \tag{4.1}$$

where f_1 represents the amplitude offorce being applied and f_2 is a constant.
substituting the assumed expressions of the field variables into the previously defined boundary conditions (4.1) yields a set of algebraic relations that must be satisfied by the associated parameters. Consequently, a system of four equations is obtained. This system is solved using the inverse matrix approach to evaluate the unknown constants $(R_1,\ R_2,\ R_3,\ \text{and } N)$ leading to explicit expressions for these quantities as given below.

$$\begin{bmatrix} R_1 \\ R_2 \\ R_3 \\ N \end{bmatrix} = \begin{bmatrix} \Theta_{51} & \Theta_{52} & \Theta_{53} & b_{12}S^2 + b_{13}\varsigma^2 \\ \Theta_{41} & \Theta_{42} & \Theta_{43} & i\varsigma\,(b_{10}-1)\,S \\ -r_1\Theta_{11} & -r_2\Theta_{12} & -r_3\Theta_{13} & 0 \\ \Theta_{21} & \Theta_{22} & \Theta_{23} & 0 \end{bmatrix}^{-1} \begin{bmatrix} 0 \\ f_1 \\ 0 \\ f_2 \end{bmatrix} \tag{4.2}$$

5. Numerical discussions and results

The analysis was applied for aluminum epoxy-like material with the following parameters and characteristics [2]

$$\begin{aligned}
j^* &= 0.196\times 10^{-4}\ \text{m}^2, \qquad \lambda = 7.59\times 10^{10}\ \frac{\text{N}}{\text{m}^2}, \qquad \rho = 2190\ \frac{\text{kg}}{\text{m}^3},\\
\mu &= 1.89\times 10^{10}\ \frac{\text{N}}{\text{m}^2}, \quad \beta_0 = 0.50\times 10^{5}\ \frac{\text{N}}{\text{m}^2.\text{K}}, \quad \lambda_0 = 0.37\times 10^{10}\ \frac{\text{N}}{\text{m}^2},\\
\beta_1 &= 0.50\times 10^{5}\ \frac{\text{N}}{\text{m}^2.\text{K}}, \quad c_e = 966\ \frac{\text{J}}{\text{kg.K}}, \quad k = 252\ \frac{\text{J}}{\text{m.s.K}}, \quad T_0 = 293^\circ\ \text{K},\\
\lambda_1 &= 0.37\times 10^{10}\ \frac{\text{N}}{\text{m}^2}, \quad a_0 = 0.61\times 10^{-10}, \quad \tau_\theta = 0.31\ \text{s}, \quad \tau_q = 0.7\ \text{s}\\
f_1 &= 1.201, \quad f_2 = 0.502.
\end{aligned}$$

In this study, numerical simulations are performed for all physical quantities at the time $t = 0.2$ over the spatial interval $0 \le z \le 5$ and along the surface $x = 2.5$. The employed numerical approach is used to investigate and describe the behavior of the displacement components u, and w, the stress components σ_{zz}, σ_{xx}, and σ_{xz}, as well as the temperature field ϑ, and the micro-elongation variable ψ. The resulting graphical results illustrate the theoretical predictions of the LST, DPLM, and RDPLM. Figures 1, 2, 3, 4, 5, 6, and 7 present a detailed comparative analysis of deterministic and stochastic field responses within the RD-PLM, highlighting the influence of random thermal fluctuations on wave propagation in a micro-elongated thermoelastic medium subjected to initial stress $(P = 2)$. Figure 1 shows the horizontal displacement distributions (u) for the RDPLM. The deterministic curve $(\nu = 0)$ displays a smooth, decaying from a large positive value. The stochastic fields $(\nu = 1, 1.1, 1.2)$ exhibit significant, chaotic, high-frequency oscillations and fluctuations, particularly near the boundary $(z \approx 0$ to $z \approx 2.5)$, indicating the greatest sensitivity of the

RDPLM to stochastic disturbances. Figure 2 clarifies the vertical displacement distributions (w) for the RDPLM. The deterministic response ($\nu = 0$) smoothly decays. The stochastic curves ($\nu = 1, 1.1, 1.2$) introduce pronounced, random oscillations across the spatial domain, confirming that random thermal fluctuations significantly modify the wave characteristics. Figure 3 depicts the stress tensor (σ_{zz}) distributions for the RDPLM. The deterministic curve ($\nu = 0$) starts negative and smoothly approaches zero. The stochastic responses ($\nu = 1, 1.1, 1.2$) show intense, high-amplitude, and random oscillations, demonstrating how initial stress effects and random thermal fluctuations significantly modify the induced stress fields and wave characteristics. Figure 4 illustrates the stress tensor (σ_{xx}) distributions for the RDPLM. The deterministic curve ($\nu = 0$) starts at a large negative value and smoothly increases toward zero. The introduction of stochasticity ($\nu = 1, 1.1, 1.2$) causes the σ_{xx} field to exhibit strong, irregular oscillations, which are most apparent near the $z \approx 0$ where thermal coupling is strongest. Figure 5 demonstrates the stress tensor (σ_{xz}) distributions for the RDPLM. The deterministic curve ($\nu = 0$) displays a smooth, wave-like pattern, starting negative, becoming positive, and then decaying to zero. The stochastic components ($\nu = 1, 1.1, 1.2$) create violent fluctuations that dominate the field response, illustrating the modification of wave propagation due to the stochastic thermal. Figure 6 shows the temperature distributions (ϑ) for the RDPLM. The deterministic response ($\nu = 0$) shows a rapid, smooth decay from a positive value at $z = 0$. The stochastic temperature fields ($\nu \neq 0$) exhibit large, sharp, and random fluctuations, as the randomness is directly introduced into the heat conduction equation. Figure 7 clarifies the micro-elongated distributions (ψ) for the RDPLM. The deterministic field ($\nu = 0$) starts negative and smoothly approaches zero with depth. Because micro-elongation is strongly coupled to temperature, the stochastic responses ($\nu \neq 0$) display intense random oscillations, highlighting the significant influence of stochasticity on the microstructural field. Figures 8, 9, 10, 11, 12, 13, and 14 provide an extensive comparison of deterministic and stochastic responses in the DPLM, demonstrating how stochastic thermal effects alter wave propagation characteristics in a micro-elongated thermoelastic medium under the influence of initial stress ($P = 2$). Figure 8 depicts the horizontal displacement distributions (u) for the DPLM. The deterministic response ($\nu = 0$) is a smooth, decaying profile. The stochastic curves ($\nu = 1, 1.1, 1.2$) introduce oscillations, but the DPLM exhibits a moderate level of sensitivity to stochastic disturbances when compared to the RDPLM. Figure 9 shows the vertical displacement distributions (w) for the DPLM. The deterministic curve ($\nu = 0$) starts negative and smoothly approaches zero. The stochastic thermal effects alter the wave propagation and introduce random oscillations and deviations from the deterministic path. Figure 10 shows the stress tensor (σ_{zz}) distributions for the DPLM. The deterministic stress starts highly negative and smoothly increases toward zero. The stochastic responses introduce significant random fluctuations, demonstrating the modification of stress distributions under initial stress and stochastic excitation. Figure 11 demonstrates the stress tensor (σ_{xx}) distributions for the DPLM. The deterministic curve starts negative and smoothly approaches zero. The stochastic components show oscillations, reinforcing the role of random thermal in modifying the stress fields. Figure 12 illustrates the stress tensor (σ_{xz}) distributions for the DPLM. The deterministic stress starts positive and smoothly decays to zero. The stochastic responses display random oscillations and deviations. Figure 13 shows the temperature distributions (ϑ) for the DPLM. The deterministic field starts positive and decays smoothly to zero. The stochastic temperature curves clarify clear random fluctuations, reflecting the impact of the Wiener process on the heat transfer process. Figure 14 clarifies the micro-elongated distributions (ψ) for the DPLM. The deterministic curve starts at a large negative value and smoothly approaches. The stochastic micro-elongation is characterized by random oscillations due to its strong coupling with the fluctuating temperature field. Figures 15, 16, 17, 18, 19, 20, and 21 display a thorough comparison between deterministic and stochastic field behaviors in the RDPL model, showing the impact of random thermal perturbations on wave propagation in a micro-elongated thermoelastic medium with an initial stress ($P = 2$). Figure 15 shows the horizontal displacement distributions (u) for the LST. The deterministic curve illustrates a large positive value at $z = 0$ that smoothly decays and oscillates around zero with increasing depth. The stochastic curves demonstrate fluctuations, but the LST demonstrates the weakest response to stochastic perturbations, consistent with its more diffusive description of heat transport. Figure16 depicts the vertical displacement distributions (w) for the LST. The deterministic response starts negative and smoothly approaches zero. The stochastic thermal effects cause random deviations from the smooth deterministic curve, though less pronounced than in the DPLM or RDPLM. Figure 17 clarifies the stress tensor (σ_{zz}) distributions for the LST. The deterministic stress starts negative and smoothly oscillates around zero. The stochastic responses introduce fluctuations that significantly change the stress, which is particularly evident near the $z = 0$ due to the effects of initial stress. Figure 18 displays the stress tensor (σ_{xx}) distributions for the LST. The deterministic curve appears a smooth wave a long the distance z. The stochastic components cause the stress field to oscillate randomly, but the LST remains the least sensitive model to these fluctuations. Figure 19 shows the stress tensor (σ_{xz}) distributions for the LST. The deterministic stress starts positive and smoothly oscillates around zero. The stochastic responses introduce random oscillations, but the fluctuations are relatively less severe compared to DPLM and RDPLM. Figure 20 exhibits the temperature distributions (ϑ) for the LST. The deterministic field displays a smooth wave-like behavior. The stochastic temperature curves show fluctuations, but the LST's diffusive description of heat transport results in the weakest response to the stochastic perturbations. Figure 21 displays the micro-elongated distributions (ψ) for the LST. The deterministic field smoothly oscillates around zero. The micro-elongation field exhibits random fluctuations for due to the thermal coupling, but this is the least prominent stochastic effect among the three models.

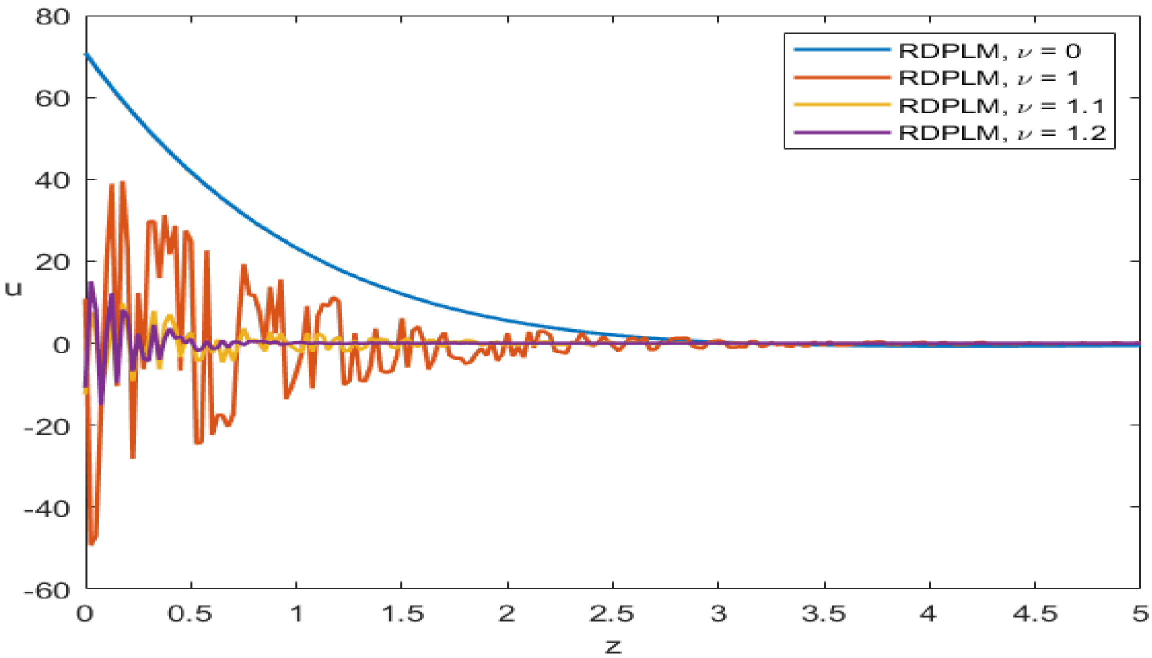

Figure 1. The horizontal displacement distributions for the RDPLM

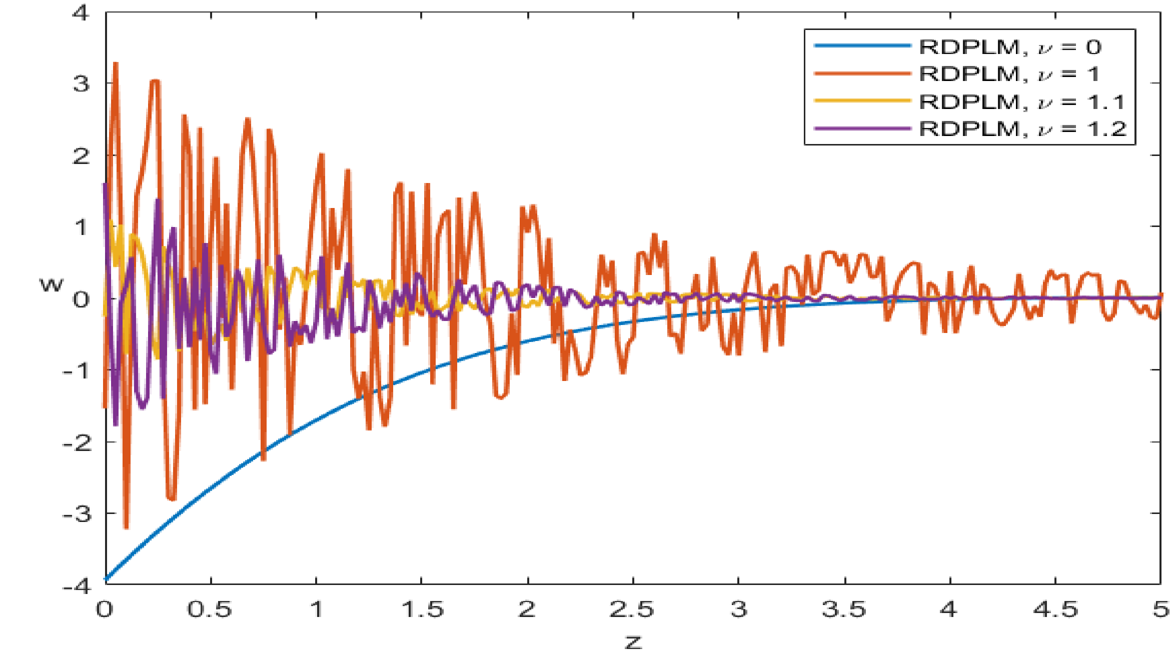

Figure 2. The vertical displacement distributions for the RDPLM

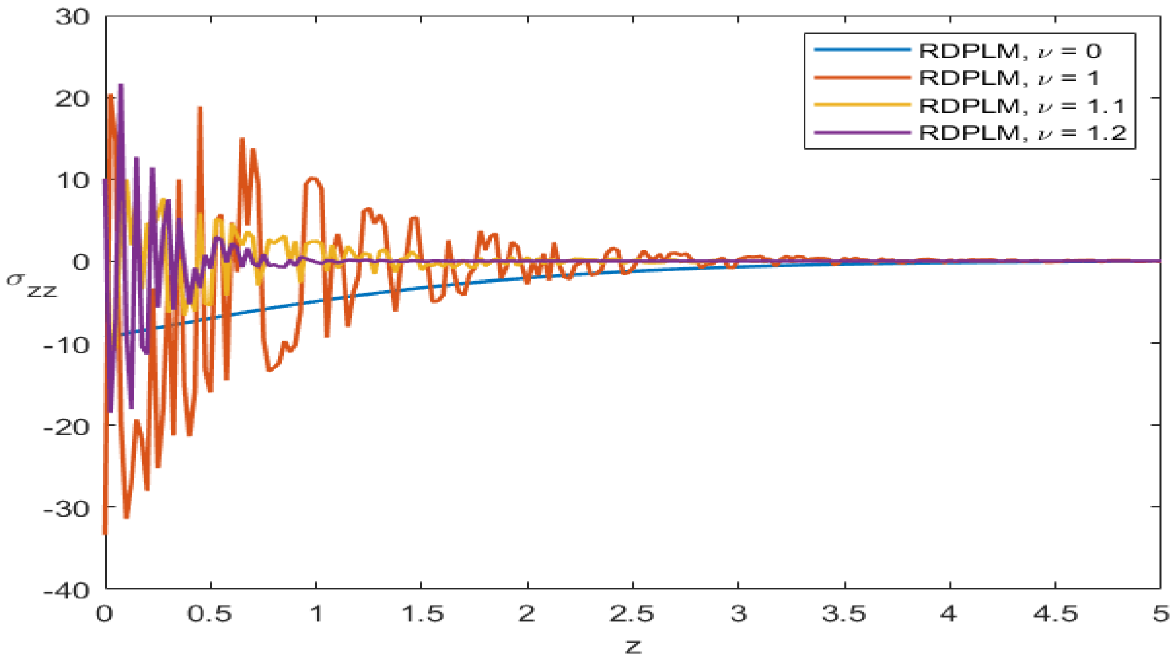

Figure 3. The stress tensor (σ_{zz}.) distributions for the RDPLM

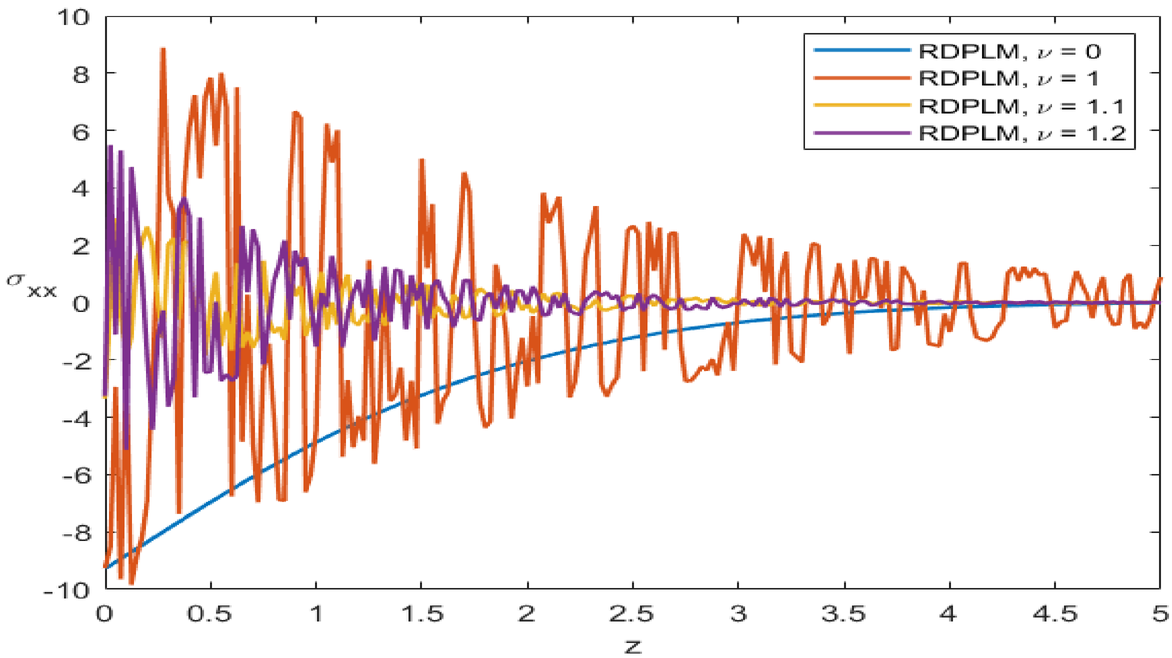

Figure 4. The stress tensor (σ_{xx}.) distributions for the RDPLM

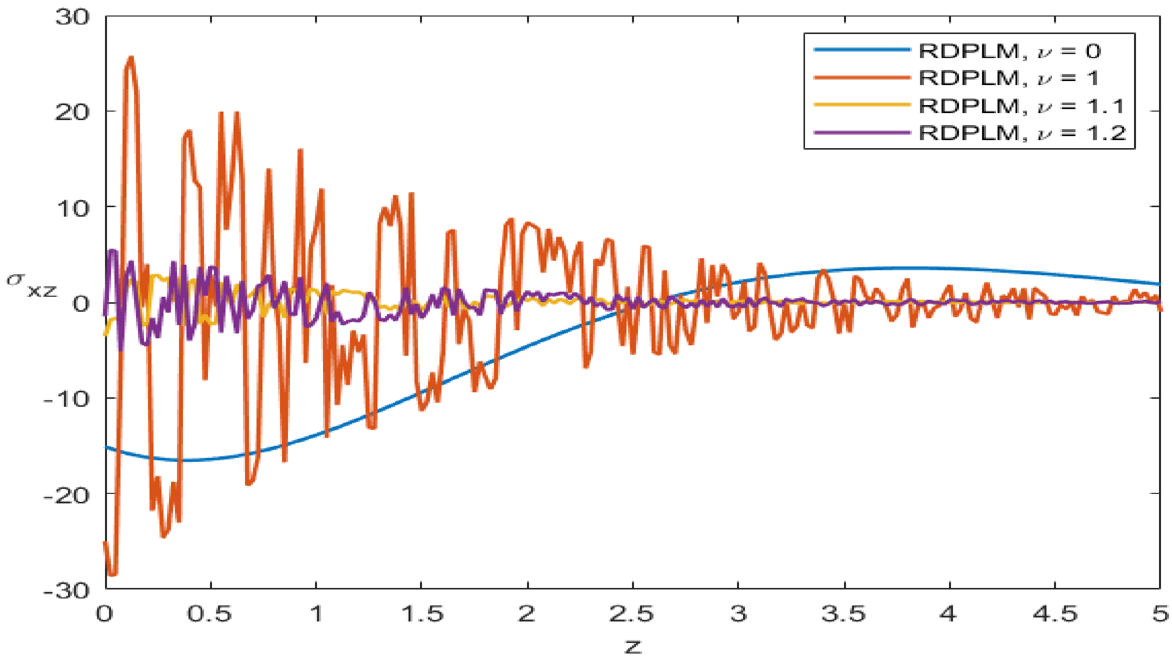

Figure 5. The stress tensor (σ_{xz}.) distributions for the RDPLM

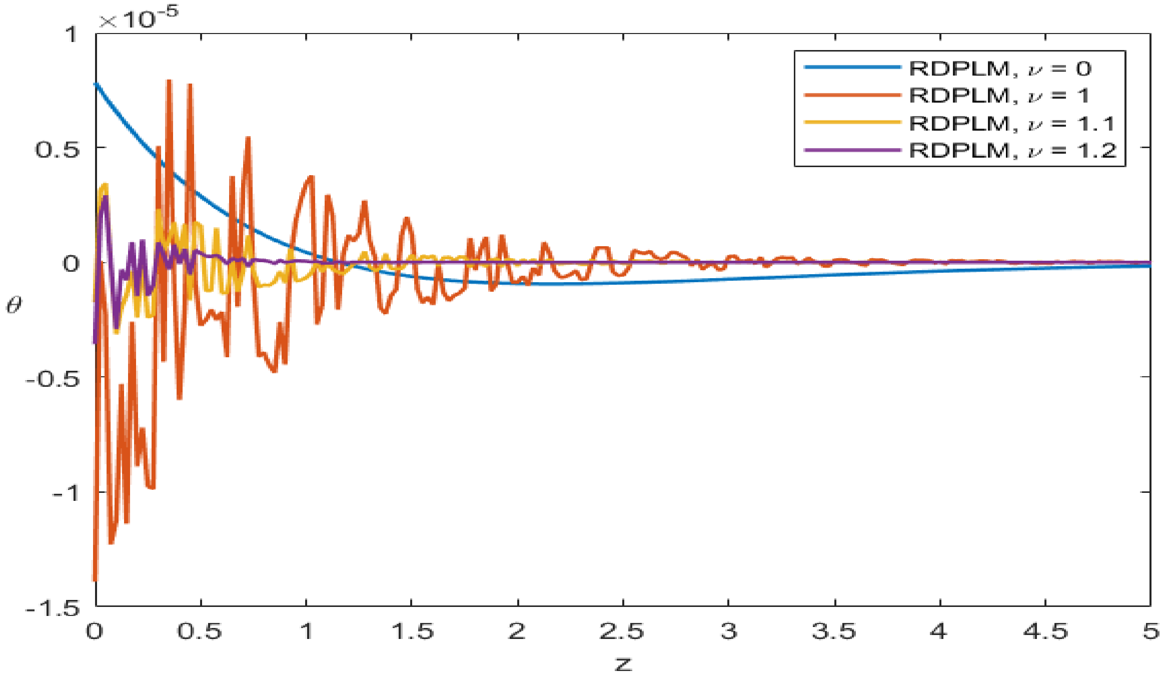

Figure 6. The temperature distributions for the RDPLM

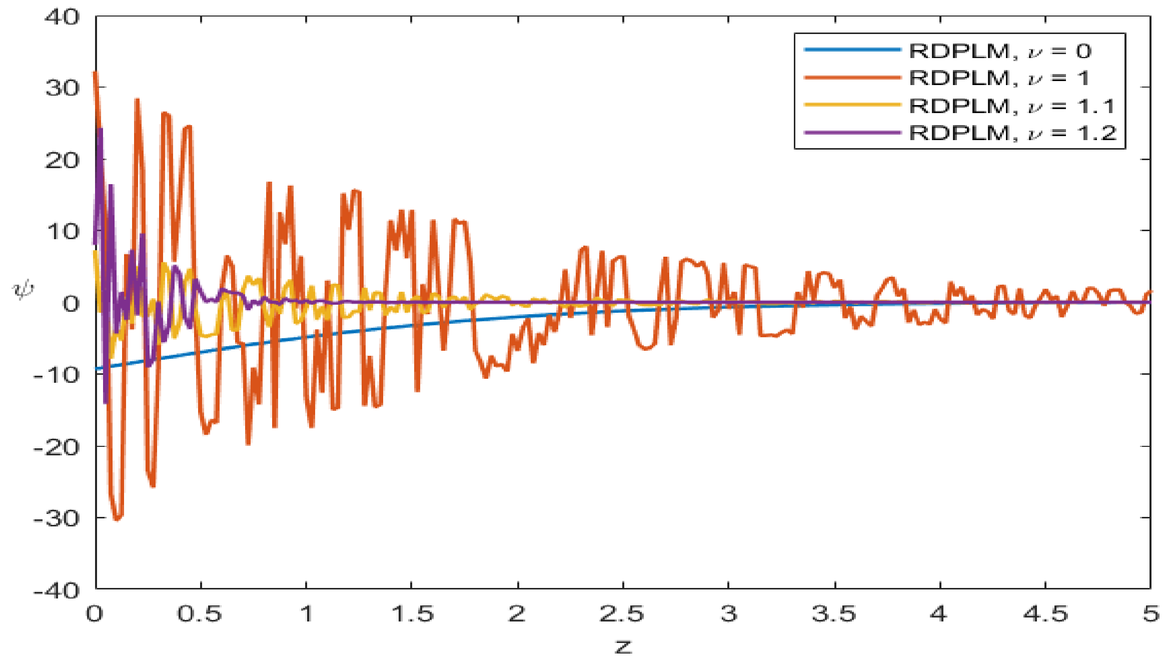

Figure 7. The micro-elongated distributions for the RDPLM

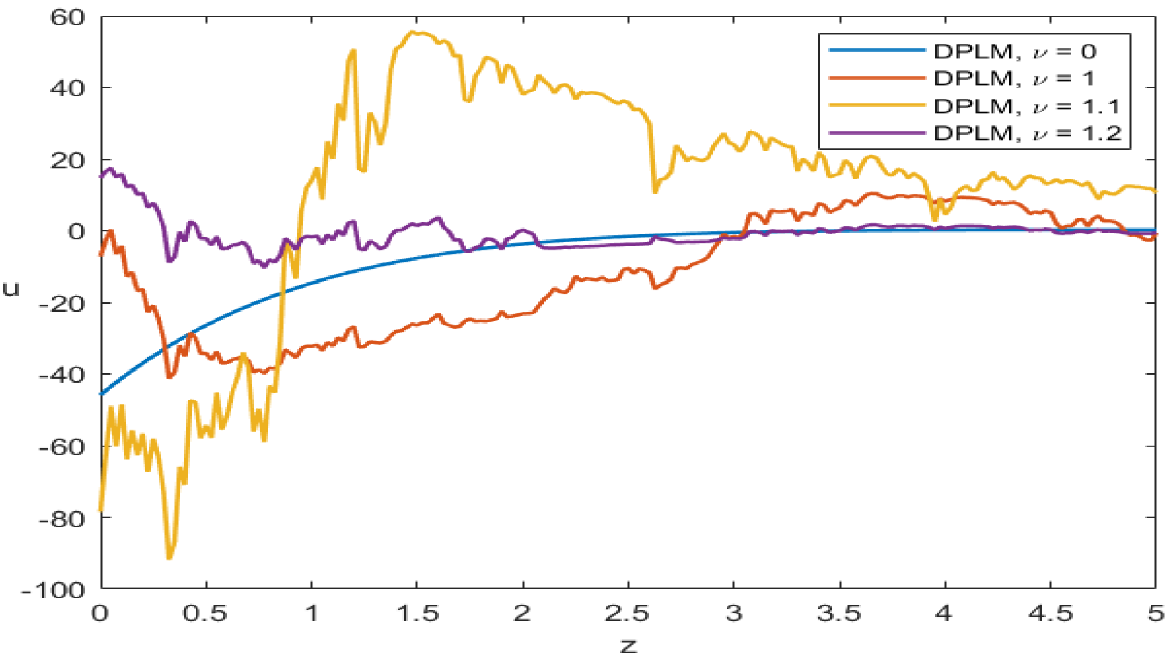

Figure 8. The horizontal displacement distributions for the DPLM

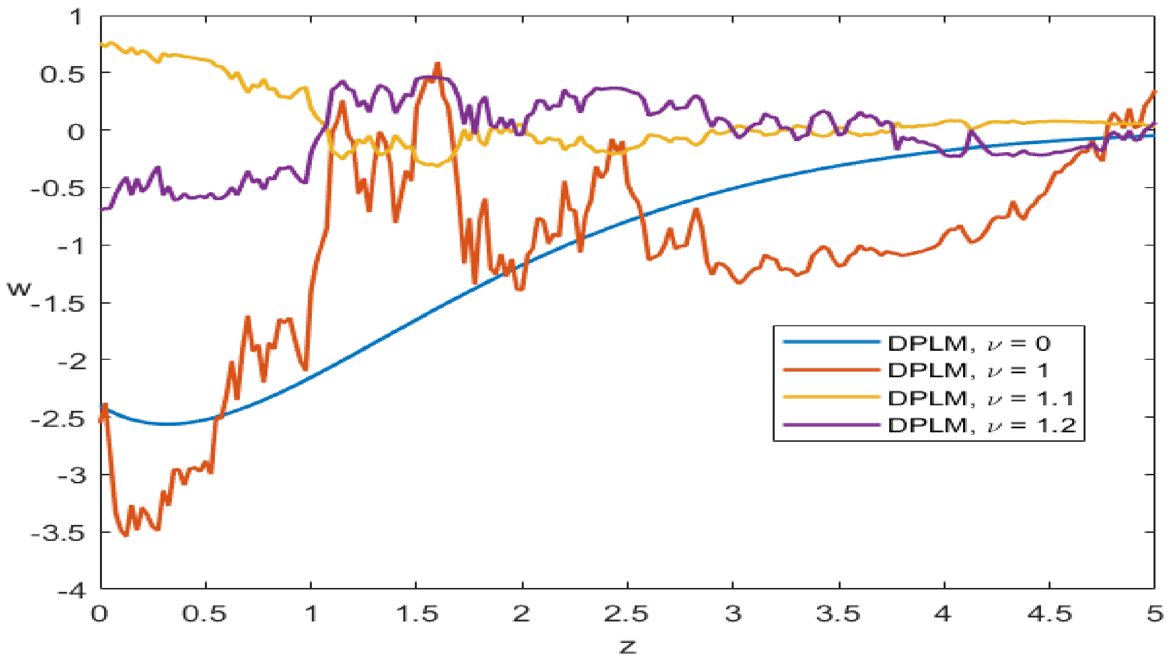

Figure 9. The vertical displacement distributions for the DPLM

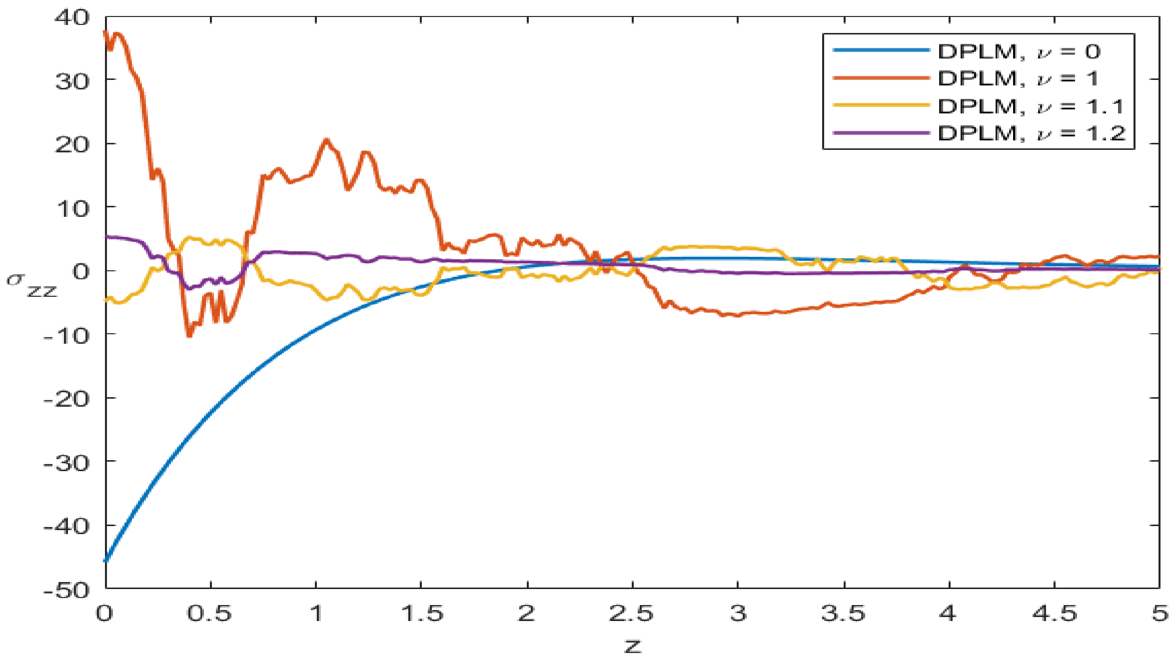

Figure 10. The stress tensor (σ_{zz}.) distributions for the DPLM

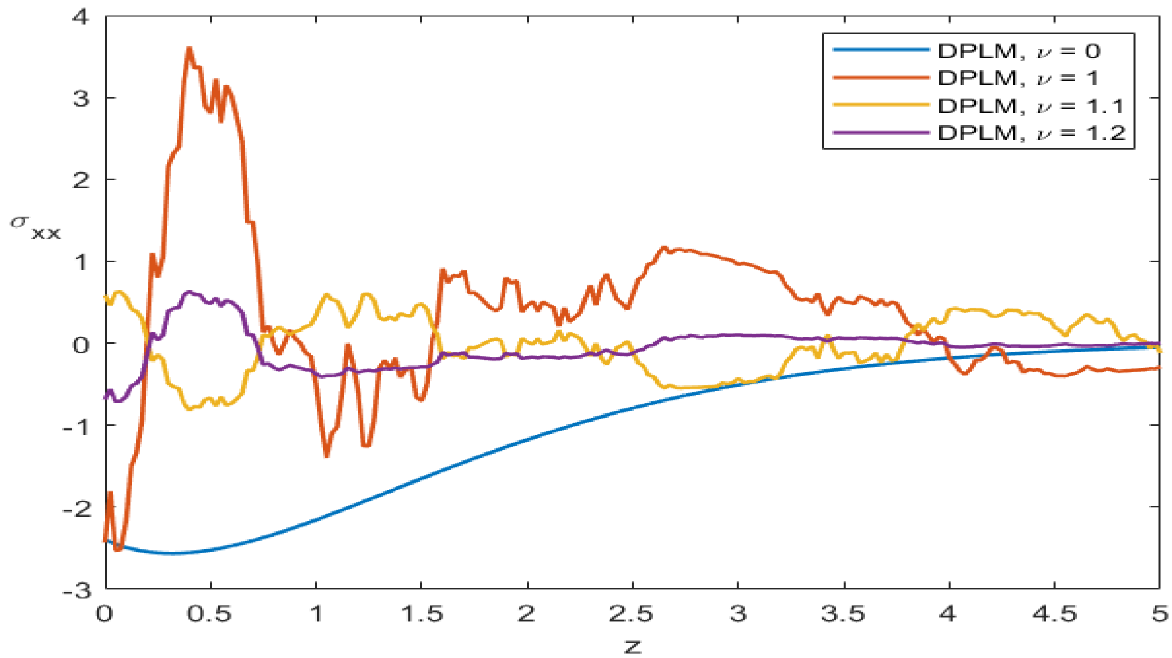

Figure 11. The stress tensor (σ_{xx}.) distributions for the DPLM

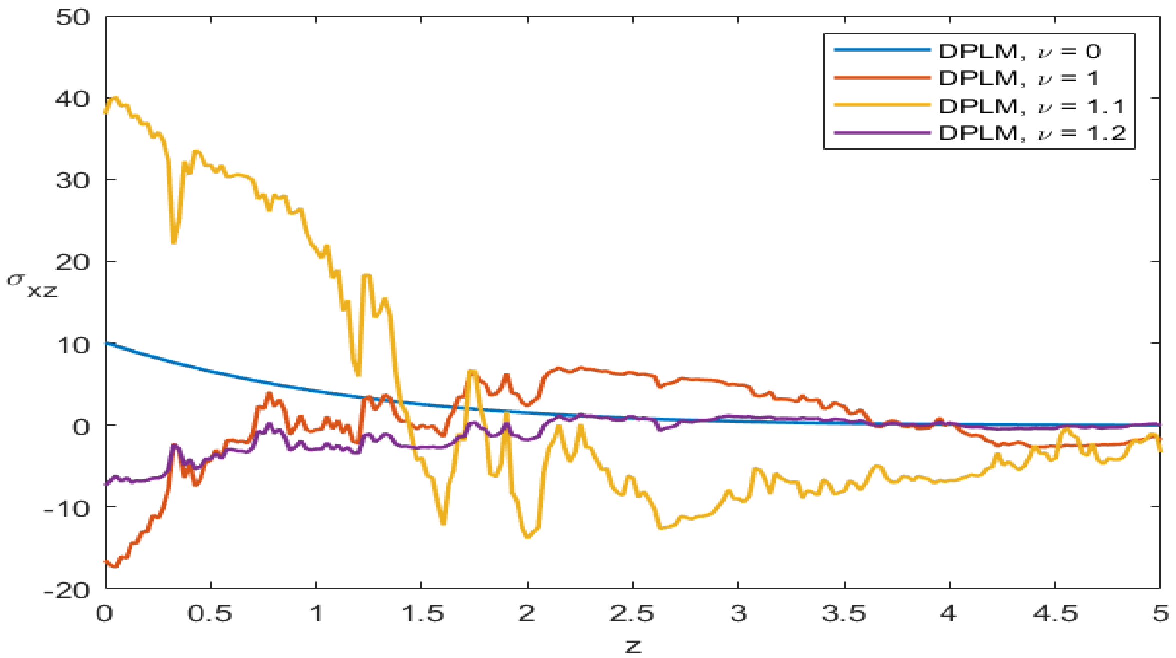

Figure 12. The stress tensor (σ_{xz}.) distributions for the DPLM

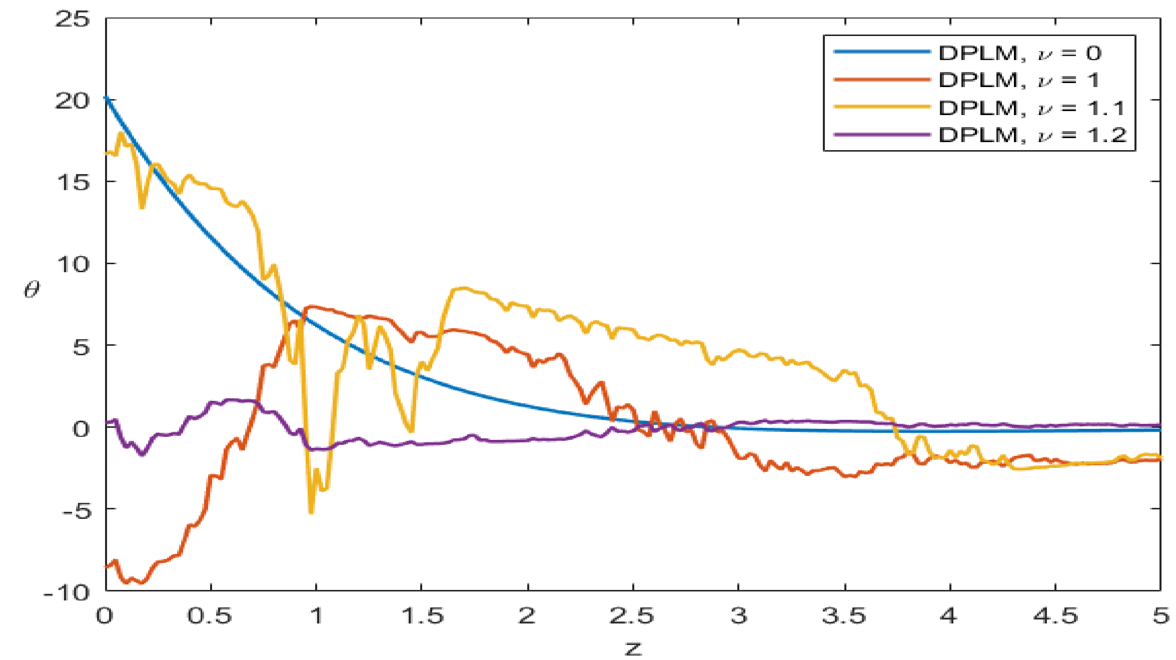

Figure 13. The temperature distributions for the DPLM

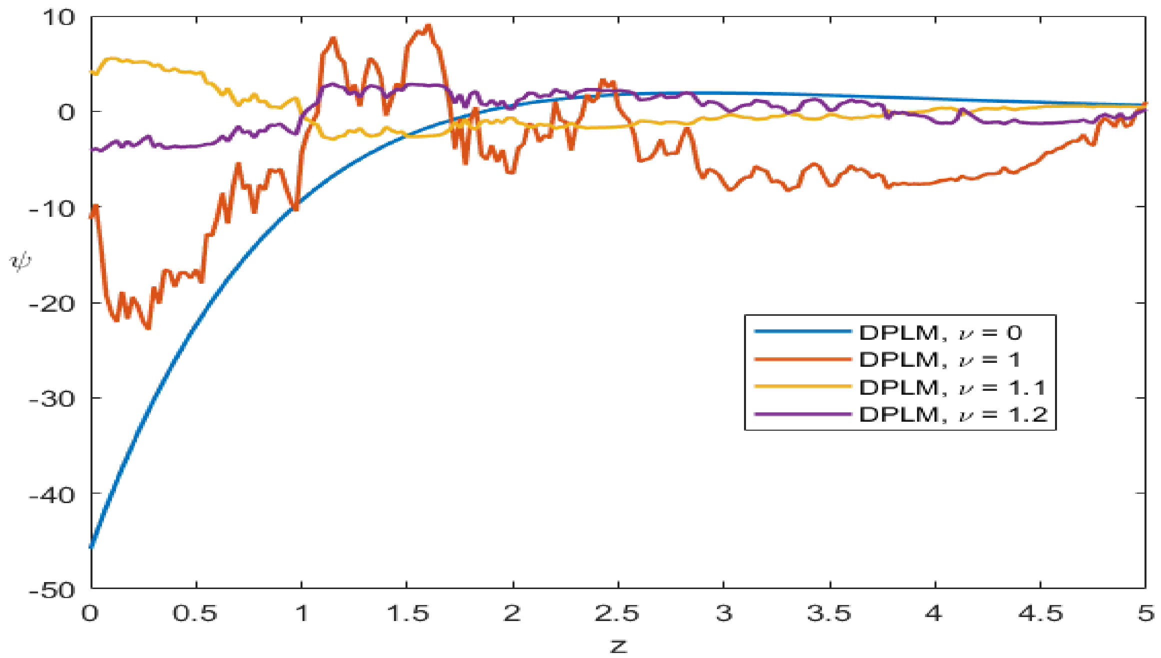

Figure 14. The micro-elongated distributions for the DPLM

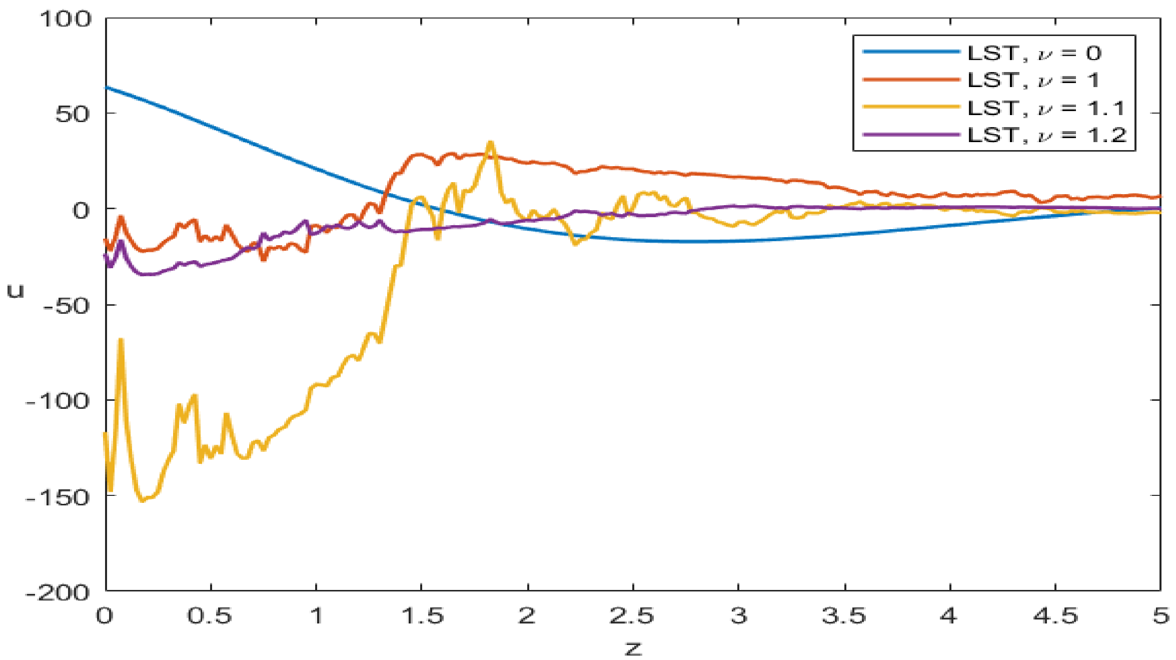

Figure 15. The horizontal displacement distributions for the LST

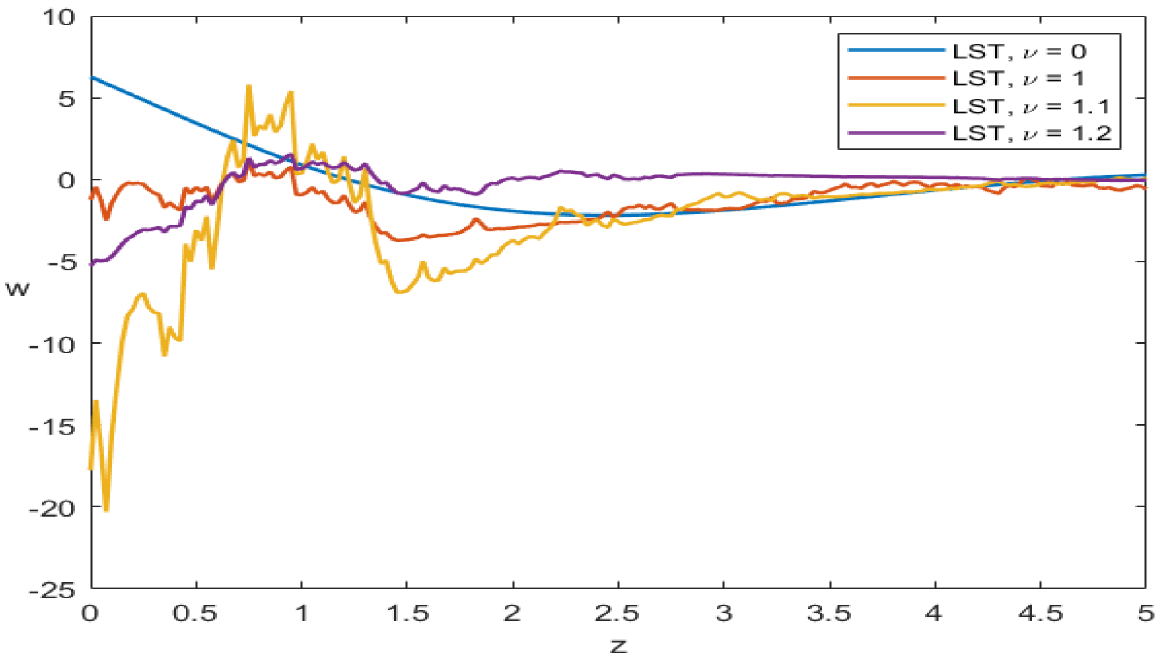

Figure 16. The vertical displacement distributions for the LST

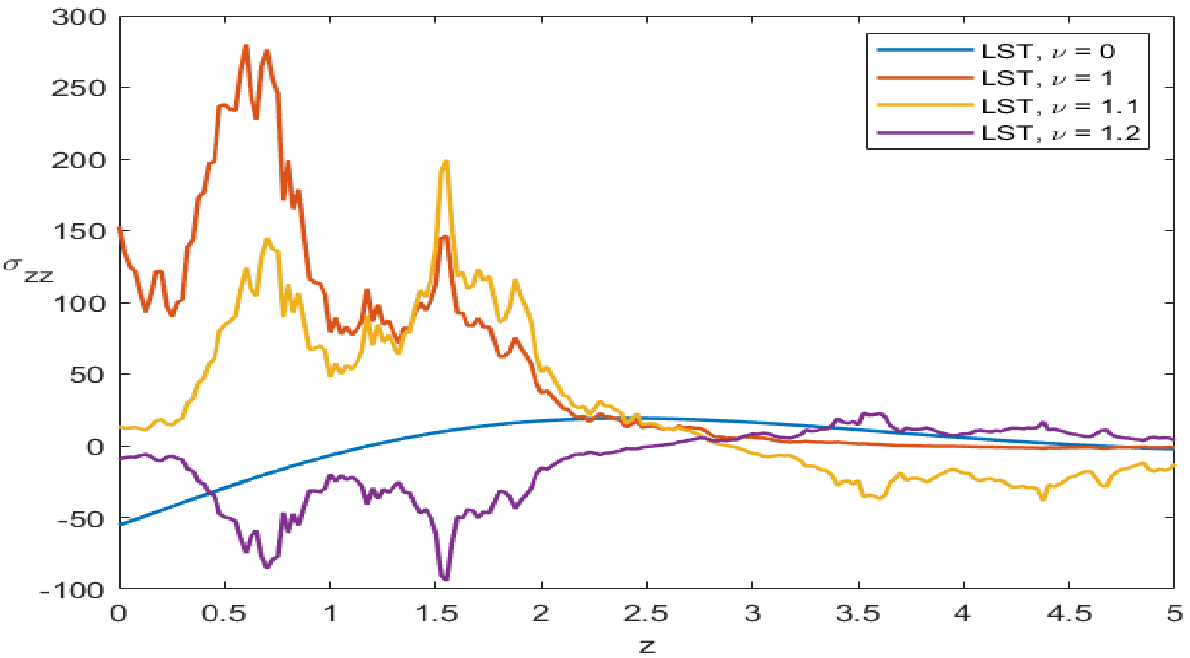

Figure 17. The stress tensor (σ_{zz}.) distributions for the LST

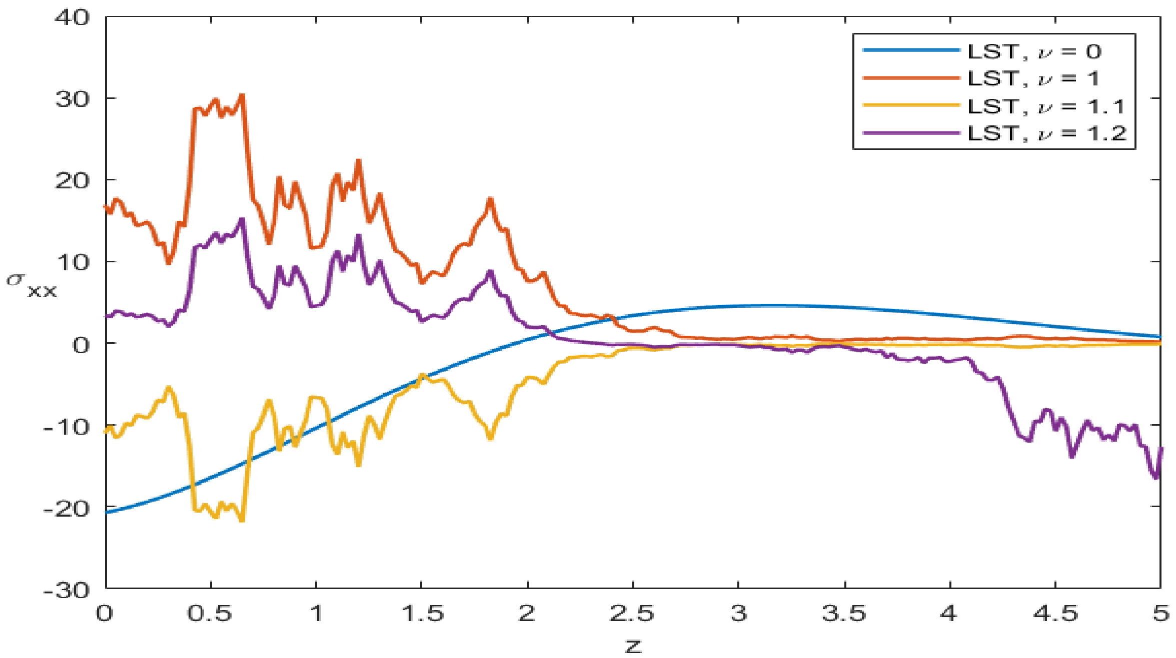

Figure 18. The stress tensor (σ_{xx}.) distributions for the LST

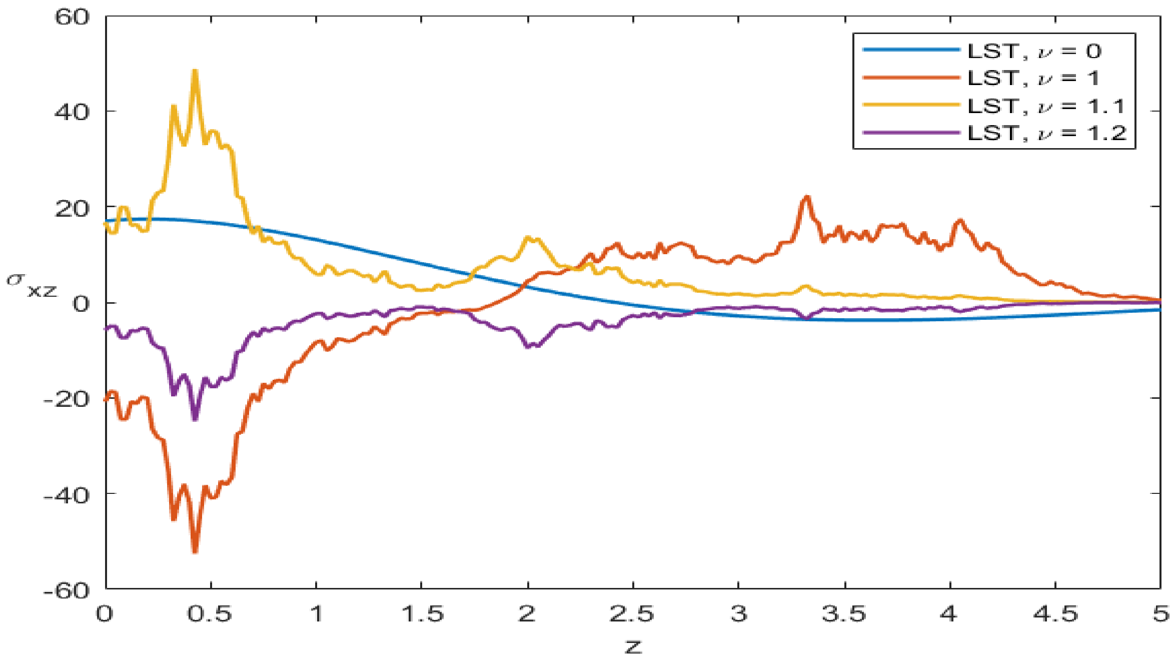

Figure 19. The stress tensor (σ_{xz}.) distributions for the LST

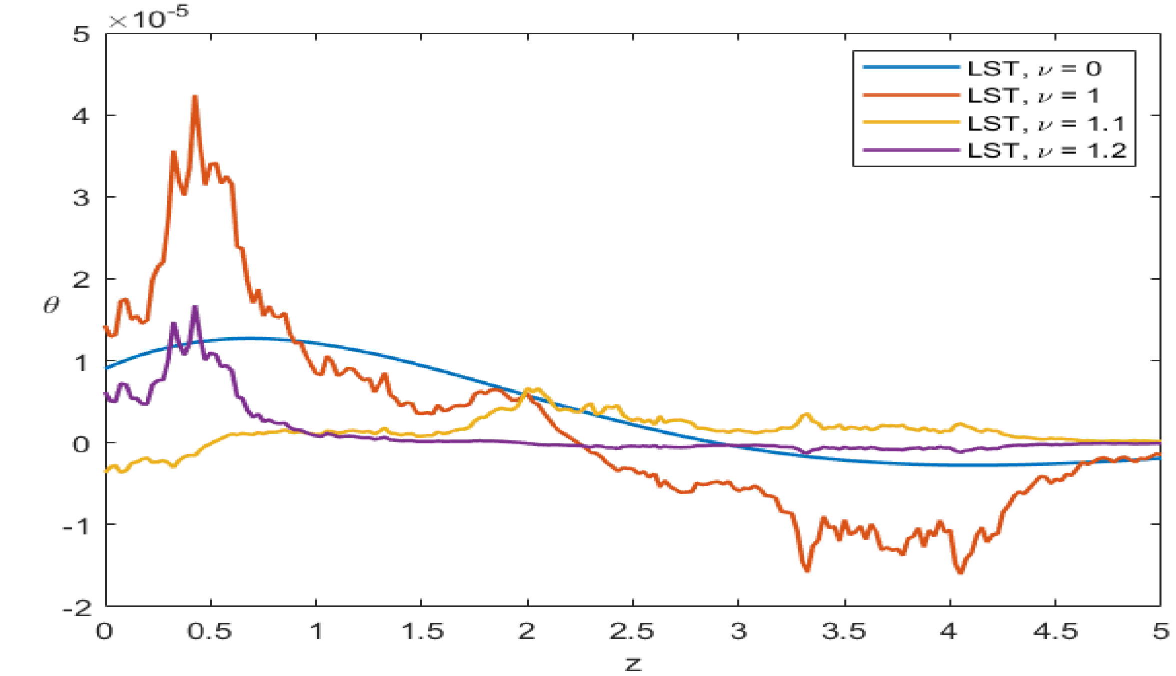

Figure 20. The temperature distributions for the LST

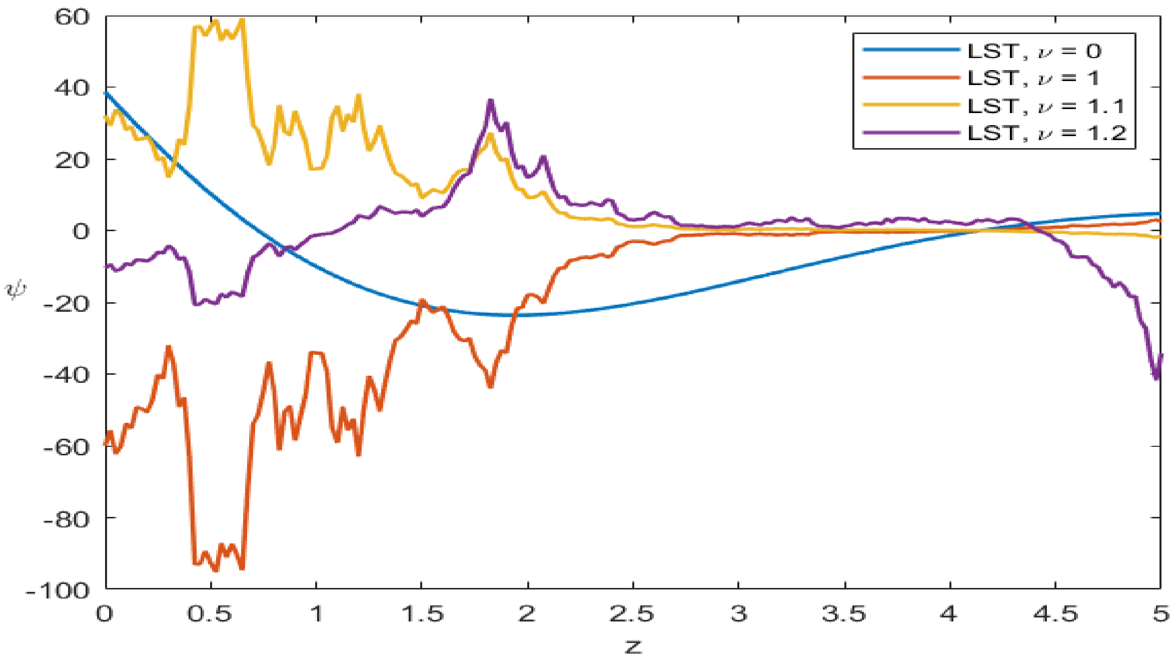

Figure 21. The micro-elongated distributions for the LST

6. Conclusion

The present investigation provides a comprehensive analytical and numerical study of the combined effects of initial stress and stochastic thermal disturbances on the propagation of coupled thermo-mechanical waves in a micro-elongated thermoelastic half-space. The analysis is performed within the frameworks of three generalized thermoelastic theories, namely the LST, the DPLM, and the RDPLM. By simultaneously accounting for the influence of pre-existing mechanical stresses and random thermal fluctuations, the developed formulation offers a more realistic representation of the behavior of advanced microstructured materials operating under uncertain thermal environments. Such a unified treatment enables the investigation of the complex interactions among mechanical deformation, heat conduction, stochastic excitation, and microstructural elongation, thereby extending the predictive capability of conventional deterministic thermoelastic models. The mathematical formulation begins with the fundamental field equations governing the coupled thermoelastic problem, including the equations of motion, generalized heat-conduction equations corresponding to each thermoelastic theory, and the evolution equation describing the micro-elongation field. These governing relations are first expressed in a unified form and subsequently simplified through suitable mathematical manipulations. By employing an appropriate integral transform technique, the original system of coupled stochastic partial differential equations is converted into a reduced system of stochastic ordinary differential equations. This transformation significantly facilitates the analytical treatment of the problem while preserving the essential coupling among the thermal, mechanical, and microstructural variables. Consequently, closed-form analytical solutions are obtained for the principal physical quantities, including the temperature distribution, displacement components, micro-elongation field, normal and shear stresses, and other related thermo-mechanical variables that characterize the response of the medium. Extensive numerical computations are then performed to evaluate the influence of the governing physical parameters and to compare the predictive capabilities of the three thermoelastic models. The numerical results reveal that the presence of initial stress has a substantial impact on the propagation characteristics of thermoelastic waves throughout the medium. Specifically, the pre-existing stress field modifies the propagation speed, amplitude, and spatial evolution of the mechanical and thermal disturbances, resulting in significant changes in the distributions of displacement, stress, temperature, and micro-elongation. These effects are particularly evident in the vicinity of the boundary surface, where the interaction between the imposed loading conditions and the initial stress field produces pronounced variations in the localized thermo-mechanical response. The results further demonstrate that both the magnitude and nature of the initial stress strongly influence the dynamic behavior of the medium, emphasizing the necessity of incorporating pre-stressed configurations into realistic thermoelastic analyses. An additional objective of the present work is to investigate the influence of stochastic thermal excitation on the coupled response of the micro-elongated medium. To accomplish this, random thermal fluctuations are introduced into the governing heat-conduction equation through a Wiener stochastic process, allowing the thermal loading to mimic the inherent randomness encountered in many practical engineering and physical systems. Compared with the corresponding deterministic solutions, the stochastic formulation generates noticeable random variations in all thermo-mechanical fields. These fluctuations are particularly significant for physical quantities that exhibit strong thermal coupling, such as the micro-elongation variable and the thermally induced stress components, where the random heat input propagates through the coupled governing equations and produces observable irregularities in both spatial and temporal responses. The obtained results clearly demonstrate that stochastic thermal effects cannot be neglected when analyzing materials operating under uncertain thermal environments, especially when microstructural interactions play a dominant role. The comparative analysis among the three generalized thermoelastic theories further illustrates the distinctive characteristics associated with each heat-conduction model. Among the investigated formulations, the RDPLM exhibits the highest degree of sensitivity to stochastic thermal disturbances. The numerical solutions obtained from this model display pronounced oscillatory patterns, sharper wave fronts, and more persistent thermal wave propagation, reflecting the model's enhanced ability to represent finite-speed heat transport together with multiple thermal phase-lag mechanisms. These characteristics enable the RDPLM to capture complex thermo-mechanical interactions that remain beyond the scope of simpler generalized thermoelastic formulations. In contrast, the DPLM predicts an intermediate response, exhibiting moderate oscillations and a balanced representation of thermal wave propagation and dissipative effects. The LST, on the other hand, demonstrates the least sensitivity to stochastic excitation because its single relaxation-time formulation leads to comparatively smoother temperature distributions and more diffusive thermal behavior, thereby suppressing the intensity of random fluctuations transmitted to the mechanical fields. Overall, the analytical and numerical findings presented in this work underscore the importance of employing higher-order generalized thermoelastic theories when investigating coupled thermo-mechanical phenomena under random thermal environments. The incorporation of multiple phase-lag effects, stochastic thermal loading, initial stress, and micro-elongation mechanisms provides a substantially more accurate description of wave propagation, stress evolution, and heat-transfer characteristics in advanced materials possessing complex internal microstructures. Consequently, the developed framework offers valuable theoretical insights into the behavior of microstructured thermoelastic media and establishes an effective foundation for future investigations involving stochastic thermoelasticity, micro-continuum mechanics, and the design of engineering materials subjected to uncertain thermal and mechanical operating conditions.

List of Nomenclatures

Quantity	Definition
$\mathbf{u}$	Displacement vector,
j^*	Microinertia,
λ and μ	Constants of Lame,
T_0	Reference temperature,
σ_{ij}	Component of stress tensor,
P	Initial stress,
λ_0, λ_1, a_0	Constants of micro-elongational,
ϑ	Temperature,
c_e	Specific heat,
ρ	Density,
t	Time,
τ_θ	Phase-lag of the temperature gradient,
k	Thermal conductivity,
ψ	Micro-elongational scalar,
α_{t_1}, α_{t_2}	Coefficient of linear thermal expansion, where $\beta_0 = (3\lambda + 3\mu)\,\alpha_{t_1}, \beta_1 = (3\lambda + 3\mu)\,\alpha_{t_2}$,
τ_q	Phase-lag of the heat flux.

Conflict of Interest

The authors declare there is no existing conflict of interest.

References

1.Abouelregal, A. E. (2021). Modified fractional thermoelasticity model with multi-relaxation times of higher order: application to spherical cavity exposed to a harmonic varying heat. *Waves in Random and Complex Media*, 31(5):812–832.

2.Ailawalia, P., Sachdeva, S. K., and Pathania, D. S. (2015). Plane strain deformation in a thermoelastic microelongated solid with internal heat source. *International Journal of Applied Mechanics and Engineering*, 20(4):717–731.

3.Ailawalia, P., Sharma, A., Marin, M., and Öchsner, A. (2024). Analysis of an initially stressed functionally graded thermoelastic medium (type iii) without energy dissipation. *Continuum Mechanics and Thermodynamics*, 36(6):1553–1564.

4.Allam, A. A., Ramadan, K. T., and Omar, M. (2016). A stochastic thermoelastic diffusion interaction in an infinitely long annular cylinder. *Acta Mechanica*, 227(5):1429–1443.

5.Alshehri, A. M., Lotfy, K., and Ibrahim, E. (2024). A novel model of microelongation thermomechanical photoacoustic waves in excited semiconductor materials. *Results in Physics*, 63:107881.

6.Ashraf, R., Amanat, F., Ashraf, F., Owyed, S., Matoog, R., Mahmoud, M., and Akgül, A. (2024). Soliton solutions for the (4+ 1)-dimensional fokas equation using integration techniques. *Alexandria Engineering Journal*, 107:61–72.

7.Bhattacharya, D. and Kanoria, M. (2024). Refined four-phase lag model for elasto-thermodiffusive interaction with harmonically varying heat sources. *Mechanics of Time-Dependent Materials*, 28(3):1853–1872.

8.Chiba, R. and Sugano, Y. (2007). Stochastic thermoelastic problem of a functionally graded plate under random temperature load. *Archive of Applied Mechanics*, 77(4):215–227.

9.Chiba, R. and Sugano, Y. (2008). Stochastic analysis of a thermoelastic problem in functionally graded plates with uncertain material properties. *Archive of Applied Mechanics*, 78(10):749–764.

10.De, A., Purkait, P., Das, P., and Kanoria, M. (2024). Memory dependent magneto-thermoelastic interaction in a rotating medium based on refined multi-phase-lag model.

11.El-Naggar, A., Kishka, Z., Abd-Alla, A., Abbas, I., Abo-Dahab, S., and Elsagheer, M. (2013). On the initial stress, magnetic field, voids and rotation effects on plane waves in generalized thermoelasticity. *Journal of Computational and Theoretical Nanoscience*, 10(6):1408–1417.

12.El-Sapa, S., Alhejaili, W., Lotfy, K., and El-Bary, A. A. (2023). Response of excited microelongated non-local semiconductor layer thermomechanical waves to photothermal transport processes. *Acta Mechanica*, 234(6):2373–2388.

13.Hafed, Z. S., Abo-Dahab, S., Kilany, A., and Ahmed, S. E. (2025). Electromagnetic field on a photothermal semiconducting voids medium under lord–shulman and refined multi-phase lag models in thermoelasticity. *International Journal of Modern Physics B*, 39(01):2550007.

14.Hilal, M. I. (2022). Thermomechanical interactions of rotating thermoelastic magneto-microelongated medium heated by laser and initially stressed via non-local elasticity and gn iii. *Acta Mechanica*, 233(12):5183–5197.

15.Hosseini, S. M. and Shahabian, F. (2011). Stochastic assessment of thermo-elastic wave propagation in functionally graded materials (fgms) with gaussian uncertainty in constitutive mechanical properties. *Journal of Thermal Stresses*, 34(10):1071–1099.

16.Kadian, P., Kumar, S., Hooda, N., and Sangwan, M. (2024a). Reflection of plane waves in a non-local viscothermoelastic half-space under variable thermal conductivity and microelongation effects. *Journal of Thermal Stresses*, 47(11):1479–1499.

17.Kadian, P., Kumar, S., and Sangwan, M. (2024b). Effect of inclined mechanical load on a rotating microelongated two temperature thermoelastic half space with temperature dependent properties. *Journal of Vibration Engineering & Technologies*, 12(3):4053–4074.

18.Khalil, E. M., Abo-Dahab, S. M., and Kilany, A. A. (2021). Electromagnetic field and initial stress on a photothermal semiconducting voids medium under thermoelasticity theories. *Mathematical Methods in the Applied Sciences*, 44(9):7778–7798.

19.Khamis, A., El-Bary, A., Lotfy, K., and Bakali, A. (2020). Photothermal excitation processes with refined multi dual phase-lags theory for semiconductor elastic medium. *Alexandria Engineering Journal*, 59(1):1–9.

20.Kumar, R., Garg, S., and Ahuja, S. (2015). Wave propagation in fibre-reinforced transversely isotropic thermoelastic media with initial stress at the boundary surface. *Journal of Solid Mechanics*, 7(2):223–238.

21.Kutbi, M. A. and Zenkour, A. M. (2022). Refined dual-phase-lag green–naghdi models for thermoelastic diffusion in an infinite medium. *Waves in Random and Complex Media*, 32(2):947–967.

22.Lotfy, K. (2026). Thermo-mechanical waves of excited microelongated semiconductor layer during photothermal transport processes. *Waves in Random and Complex Media*, 36(1):690–706.

23.Lotfy, K., Ahmed, A., El-Bary, A., El-Shekhipy, A., and Tantawi, R. S. (2022). A novel stochastic photo-thermoelasticity model according to a diffusion interaction processes of excited semiconductor medium. *The European Physical Journal Plus*, 137(8):972.

24.Lotfy, K., Ahmed, A., El-Bary, A. A., Tantawi, R. S., Elidy, E. S., Saeed, A. M., and Mahdy, A. (2024). A stochastic photoacoustic study influenced by white noise on thermoelastic waves in semiconductor medium. *Semiconductors*, 58(12):948–959.

25.Mohammed, W. W., Cesarano, C., Alqsair, N. I., and Sidaoui, R. (2024). The impact of brownian motion on the optical solutions of the stochastic ultra-short pulses mathematical model. *Alexandria Engineering Journal*, 101:186–192.

26.Rezk, E. G., Ismail, G. M., Ahmed, A., Lotfy, K., El-Bary, A. A., Can, E., and Elidy, E. (2025). A stochastic dual-phase-lag two-temperature photo-thermoelastic model for double-porosity semiconductors with initial stress. *Scientific Reports*.

27.Sherief, H. H., El-Maghraby, N. M., and Allam, A. A. (2013). Stochastic thermal shock problem in generalized thermoelasticity. *Applied Mathematical Modelling*, 37(3):762–775.

28.Sherief, H. H., El-Maghraby, N. M., and Allam, A. A. (2017). Stochastic thermal shock problem and study of wave propagation in the theory of generalized thermoelastic diffusion. *Mathematics and Mechanics of Solids*, 22(9):1767–1789.

29.Ullah, N., Asjad, M. I., Awrejcewicz, J., Muhammad, T., and Baleanu, D. (2022). On soliton solutions of fractional-order nonlinear model appears in physical sciences. *Aims Math*, 7(5):7421–7440.

30.Zenkour, A. M. (2020). Thermo-diffusion of solid cylinders based upon refined dual-phase-lag models. *Multidiscipline Modeling in Materials and Structures*, 16(6):1417–1434.

31.Zenkour, A. M., Saeed, T., and Aati, A. M. (2023). Refined dual-phase-lag theory for the 1d behavior of skin tissue under ramp-type heating. *Materials*, 16(6):2421.

© 2026 by the authors. Disclaimer/Publisher's Note: The content in all publications reflects the views, opinions, and data of the respective individual author(s) and contributor(s), and not those of Sphinx Scientific Press (SSP) or the editor(s). SSP and/or the editor(s) explicitly state that they are not liable for any harm to individuals or property arising from the ideas, methods, instructions, or products mentioned in the content.